forests

MDPI

Article

Physiological, Transcriptomic and Metabolomic Analyses of Overwintering *Cryptomeria fortunei* Needles

Yingting Zhang [1,2,3], Hailiang Hu [1,2,3], Junjie Yang [1,2,3], Jinyu Xue [1,2,3] and Jin Xu [1,2,3,*]

[1] Key Laboratory of Forest Genetics & Biotechnology of Ministry of Education, Nanjing Forestry University, Nanjing 210037, China
[2] Co-Innovation Center for Sustainable Forestry in Southern China, Nanjing Forestry University, Nanjing 210037, China
[3] College of Forestry, Nanjing Forestry University, Nanjing 210037, China
* Correspondence: xjinhsh@njfu.edu.cn; Tel.: +86-25-8542-7319

Abstract: Low temperatures affect plant growth, development, and geographical distribution. *Cryptomeria fortunei* (Chinese cedar) is a major industrial tree species used for timber manufacturing in southern China. However, its popularization and application in northern China are limited due to its poor low-temperature resistance (approximately −6 °C), and its overwintering mechanism remains unclear. Here, we performed physiological, metabolomic, and transcriptomic analyses of overwintering *C. fortunei* needles at three stages: before winter, during winter, and in early spring. Physiological analyses showed that electrolyte leakage, H_2O_2, malondialdehyde (MDA), soluble sugar, and protein contents increased, while the maximum quantum yield of photosystem II (PSII) (F_v/F_m), effective quantum yield of PSII (Y_{II}), and chlorophyll content decreased as overwintering progressed. Metabolomic and transcriptomic analyses revealed that downregulated gibberellin (GA), salicylic acid (SA), cytokinin (CTK), and auxin signal transduction and upregulated abscisic acid (ABA), ethylene, brassinosteroids (BR), and jasmonic acid (JA) signal transduction pathways promoted the winter acclimation of *C. fortunei*, while the opposite expression pattern promoted the transition from dormancy to growth. In addition, upregulated genes/metabolites involved in phenylpropanoid and flavonoid biosynthesis, starch and sucrose metabolism, cold-related protein and fatty acid desaturases, and downregulated photosynthesis-related pathways promoted winter acclimation, while five (*WRKY*, *AP2/ERF*, *NAC*, *MYB*, and *bHLH*) and three (*AP2/ERF*, *MYB*, and *bHLH*) transcription factors were associated with winter acclimation and early spring transition from dormancy to growth, respectively. In summary, we report the first transcriptome of overwintering *C. fortunei*, providing a foundation for the cultivation of and research on overwintering varieties.

Keywords: overwintering mechanism; transcriptome; LC-MS; starch and sucrose metabolism; plant hormone signal transduction; cold-related protein; fatty acid desaturase; transcription factor

check for updates

Citation: Zhang, Y.; Hu, H.; Yang, J.; Xue, J.; Xu, J. Physiological, Transcriptomic and Metabolomic Analyses of Overwintering *Cryptomeria fortunei* Needles. *Forests* **2022**, *13*, 1249. https://doi.org/10.3390/f13081249

Received: 8 June 2022
Accepted: 4 August 2022
Published: 7 August 2022

Publisher's Note: MDPI stays neutral with regard to jurisdictional claims in published maps and institutional affiliations.

Copyright: © 2022 by the authors. Licensee MDPI, Basel, Switzerland. This article is an open access article distributed under the terms and conditions of the Creative Commons Attribution (CC BY) license (https://creativecommons.org/licenses/by/4.0/).

1. Introduction

Cryptomeria fortunei (Chinese cedar), an endemic tree species in China, is widely distributed in southern China [1]. Due to its beautiful tree shape, fast growth, and excellent wood materials, it has good ornamental and economic value. However, its growth, development, and spatial distribution are adversely affected by low temperature (LT) in winter due to its poor LT resistance (Lethal temperature for 50% (LT_{50}) is approximately −6 °C [2]); therefore, it is difficult to widely cultivate this species in northern China. To date, research on the LT resistance of *Cryptomeria* has mainly focused on physiology [2,3], and the related molecular mechanism in this genus is poorly understood. Therefore, clarifying the LT acclimation mechanism of overwintering *C. fortunei* is very important for improving its tolerance to winter climates via breeding in the future.

LT is the most important environmental stress factor in the Yangtze River Basin (including Nanjing, Jiangsu, China) of China in winter. It is one of the most important abiotic

stresses affecting plant health globally and is also one of the most serious environmental pressures that restricts plant growth, development, yield, and geographic distribution [4]. LT stress results in a variety of observable or measurable damage symptoms, including visible necrosis of specific tissues and organs and even death of the entire plant, or less obvious cellular symptoms, as measured by osmotic reactivity, sub-display microstructural observations, chlorophyll fluorescence, and relative electrolyte leakage (REL) in affected tissues [2,5,6]. A general symptom of cellular injury is a loss of plasma membrane semi-permeability, resulting in the release of intracellular electrolytes; therefore, REL is widely used to measure changes in LT tolerance [6–8]. Studies have shown that a certain degree of cold acclimation effectively improves plant resistance to LT stress [9]. In general, plants can improve LT resistance mainly through the following strategies: enhancing protective enzyme activities and osmotic regulation systems, improving photosynthetic pigment contents and photosynthesis, upregulating the expression of multiple LT tolerance genes through *dehydration-responsive element-binding* (*DREB*)/*C-repeat binding factor* (*CBF*) transcription factors (TFs), and regulating Ca^{2+} and hormones via genes induced by LT [10–13]. Specifically, lipids, unsaturated fatty acids, soluble proteins (SPs), protective enzymes, soluble sugars, and free proline increase under LT stress, protecting cells against the stress. Similarly, plant pigments and photosynthesis-related indicators, such as chlorophyll (chl) content, the photosynthetic rate, stomatal conductance, the transpiration rate, and the maximum quantum yield of photosystem II (PSII) (F_v/F_m), generally decline under LT stress, reducing photosynthetic efficiency [2]; if these parameters are improved by genetically modified methods, LT resistance can be significantly improved [14]. TFs play a key regulatory role in the LT response, as they can directly or indirectly regulate the expression of a series of related genes downstream [15–18]. To date, many TFs have been reported to be involved in the plant LT response, such as *apetala2/ethylene-responsive factor* (*AP2/ERF*), *NAM*, *ATAF1/2 and CUC2* (*NAC*), *v-myb avian myeloblastosis viral oncogene homolog* (*MYB*), and *basic helix-loop-helix* (*bHLH*), which have been well studied [19–22]; among them, the *CBF* TFs in the *AP2/ERF* family play an important role in the LT response, and research on this family has mainly focused on the regulatory mechanism of the LT response induced by *inducer of CBF expression 1 (ICE1)-CBF*s that relies on *CBF* [23–25]. The role of abscisic acid (ABA) in plant LT resistance has been widely confirmed, and a rapid increase in the level of endogenous ABA will activate specific signaling pathways and change gene expression levels to enhance LT resistance [26,27]. Therefore, in view of these regulatory mechanisms, the overwintering process of plants may involve multiple genes, and their multilevel regulatory network is complex.

In the natural environment, light is also the main factor affecting plant growth and overwinter survival; it may lead to photo-oxidative damage in plants and stimulate light-damage defense mechanisms [28,29]. Studies have found that the reddening of leaves of overwintering evergreen plants mainly occurs on the light-facing side of sunny leaves under a strong light environment [3,30]. LT in winter does not affect the capture of light energy in leaves but reduces the activity of enzymes involved in the Calvin cycle in leaf photosynthesis [31], resulting in an imbalance between light energy absorption and utilization [32,33]. In the case of persistent excess light energy, the overexcited excess electrons in chl transfer single electrons to ground-state oxygen through some components in the electron transport chain, eventually leading to the synthesis of a large amount of reactive oxygen species (ROS) [34,35]. In addition, LT and high light environment promotes anthocyanin synthesis. For example, Nozzolillo et al. [36] found that under high light, the leaf anthocyanin content of Jack pine (*Pinus banksiana*) seedlings exposed to 5 °C was threefold higher than that exposed to 15 °C. Therefore, a large amount of ROS generated under extreme LT and high light in winter may be one of the key factors causing the reddening of sun leaves of evergreen plants, and it may also play an important role in the synthesis of leaf anthocyanins.

In recent years, with the rapid development of technologies such as genomics and bioinformatics, high-throughput sequencing technology has become more mature. RNA-

sequencing (RNA-seq) technology has the advantages of simplicity, low cost, high accuracy, sensitivity to gene expression abundance, and the ability to quickly identify and analyze large amounts of data. These advantages make it possible to quickly and efficiently analyze RNA transcription profiles under given conditions [37]. RNA-seq has been successfully applied to transcriptome studies of many LT-exposed plants or plant tissues, such as bell peppers (*Capsicum annuum*) [38], pomegranate (*Punica granatum*) [39], Siberian pine (*Pinus sibirica*) [40], broad-leaved Korean pine (*Pinus koraiensis*) [41] and Norway spruce (*Picea abies*) [42]. In the plant LT stress response, the expression of genes encoding cold-related transcription factors (such as *bHLH*, *NAC*, and *AP2/ERF*) and genes involved in the perception and transmission of cold signals, antioxidant defenses, osmotic regulation and photosynthesis changed significantly [40–42]. In addition, proteomic and metabolomic approaches have also been used to identify changes in proteins and metabolites involved in the cold acclimation process of conifers [6,7,43,44]. The accumulation of carbohydrates including oligosaccharides from the raffinose family, sugar acids and sugar alcohols, desaturation of fatty acid and changes in lipid composition, accumulation of protein, non-protein amino acids, and polyamines were observed during winter cold acclimation [5,6,43]. In general, cold tolerance is co-regulated by multiple genes, proteins, and metabolites, such as cold response gene (*COR*), lipid transfer and degradation protein (glycerol-3-phosphate acyltransferases, *GPAT*; lipid transfer protein, LTP), fatty acid desaturase (*FAD*), and late embryogenesis abundant protein (LEA) [45]. Although transcriptomic, proteomic, and metabolic changes have been studied in cold-tolerant conifer species, less cold-tolerant conifer species have not been well-studied. To date, no research involving the overwintering molecular mechanisms of *C. fortunei* has been reported.

In the present study, we measured physiological indicators and performed metabolomic and transcriptomic analyses of overwintering *C. fortunei* needles at three stages: before winter, during winter, and in early spring. Based on these data, we propose a regulatory network of overwintering *C. fortunei*. This study is the first to report the molecular mechanism underlying overwintering in *C. fortunei*, which provides a reference for strengthening its resistance through genetic improvement.

2. Materials and Methods

2.1. Plant Materials

Five-year-old *C. fortunei* seedlings cultivated in the Garden of Experimental Teaching Center of Nanjing Forestry University (32°04′41″ N, 118°48′43″ E, Jiangsu, China) were used as experimental materials. At three stages, i.e., in late autumn (LA, 28 November 2019; monthly average temperature 13.10 °C; actual sampling temperature 10 °C), winter (W, 28 December 2019; monthly average temperature 6.97 °C; actual sampling temperature 8 °C), and early spring (ES, 15 February 2020; monthly average temperature 8.10 °C; actual sampling temperature 6 °C) [46], the upper-middle or upper needles of the secondary branches were collected from 14:00 to 15:00. For each sampling stage, samples from three different trees were taken as three biological replicates. For the physiological and metabolomic analysis, three biological samples in duplicate (6 samples for one sampling period) were taken, but for transcriptomic analysis three biological samples in single (3 samples for one sampling period) were taken. Part of the samples were directly used to measure physiological indicators (i.e., electrolyte leakage (EL), water content, and chl content), and the others were immediately placed in liquid nitrogen and transferred to storage at −80 °C for further use.

2.2. Physiological Parameter Determination

The physiological parameters of *C. fortunei* needles, including EL, relative water content, soluble sugar, soluble starch, malondialdehyde (MDA), hydrogen peroxide (H_2O_2) and soluble proteins (SP) contents, chl contents, chl fluorescence, and the activities of peroxidase (POD) and superoxide dismutase (SOD), were measured.

EL was measured using a conductivity meter (DDS-307, Leici Instruments Co.; Shanghai, China) based on the method of Tsarouhas et al. [47]. A 0.2 g needle sample was placed in a centrifuge tube and incubated for 12 h with 20 mL of distilled water at 25 °C. The conductivity at this time was denoted E_1 by setting the conductivity of the distilled water to E_0. The sample was boiled for 20 min, cooled to 25 °C (placed at room temperature for 2 h) and shaken well, and the conductivity was measured as E_2. EL was then calculated using the following formula: EL (%) = $(E_1 - E_0)/(E_2 - E_0) \times 100$. One gram of needle material was dried to a constant weight at 105 °C for 48 h and was determined as M, and the water content (%) was calculated using the following formula: water content (%) = $(1 - M) \times 100\%$. The contents of soluble sugar and starch were determined by anthrone colorimetry at 630 nm [48]. The chl content was determined using the 96% ethanol extraction method according to Lichtenthaler and Wellburn [49]. A 0.1 g sample was ground with calcium carbonate, quartz sand, and ethanol, and then the optical density (OD) was measured at 665 and 649 nm wavelengths using a spectrophotometer (V-1200, Shanghai Mapada Instruments Co., Ltd.; Shanghai, China) after centrifugation at 5000 rpm at 4 °C for 20 min (Allegra X-22R, Beckman Coulter, Inc.; Breabbe, CA, USA). A DUAL-PAM-100 (Walz, Effeltrich, Baden-Wuertenberg, Germany) was used to detect chl fluorescence in dual-channel mode (fluo + P700) at a saturating light intensity of 3500 μmol m^{-2} s^{-1} along with actinic light (300 μmol m^{-2} s^{-1}) after 20 min of dark adaptation [50]. The fluorescence signal was stable for 5 min under photochemical conditions, and the following two parameters were selected as evaluation indexes for the physiological conditions of photosynthesis: F_v/F_m and the effective quantum yield of PSII (Y_{II}). Y_{II} reflects the current effective light energy conversion efficiency of the photosynthetic machinery.

Needles (0.3 g) ground with 2.7 mL of 50 mM prechilled Tris-HCl buffer (pH 7.4) were used for the determination of antioxidant enzymes and other indicators. MDA and SP contents were measured using the thiobarbituric acid method [51] and Coomassie brilliant blue G-250 method [52], respectively. POD activity and H_2O_2 content were determined at 470 nm according to the method described by Britton and Maehly [53] and Li et al. [48], respectively, and one activity unit was defined as an absorbance change of 0.01 units per min. SOD activity was measured based on the method of Giannopolites and Ries [54], and an enzyme activity unit was defined as the amount of enzyme required to inhibit 50% of the NBT reduction rate measured at 560 nm. Each indicator had six biological replicates.

2.3. RNA Extraction and cDNA Library Construction

Total RNA was extracted using RNeasy Plant Mini Kits (Qiagen, Hilden, North Rhine-Westphalia, Germany) according to the manufacturer's protocol. The length and quality inspections of RNA samples were performed using an Agilent 2100 Bioanalyzer (Agilent Technologies, Santa Clara, CA, USA), and the samples with RNA integrity numbers (RINs) ≥ 7.0 and 28S/18S ≥ 0.7 were used for subsequent experiments. Then, 9 cDNA libraries were constructed by OE Biotech Co., Ltd. (Shanghai, China), and sequenced on an Illumina HiSeq 2500 instrument.

2.4. Transcriptomic Analysis

Raw reads were subjected to quality control to obtain high-quality clean reads by removing adaptors, low-quality bases, and N-bases using Trimmomatic v0.36 [55]. These clean reads were spliced to obtain transcript sequences based on the paired-end splicing method using Trinity v2.4 [56], and then the longest one was selected as a unigene according to sequence similarity and length. These selected unigenes were compared with the nonredundant (NR), Eukaryotic Orthologous Groups of proteins (KOG), Gene Ontology (GO), Swiss-Prot, evolutionary genealogy of genes, Nonsupervised Orthologous Groups (eggNOG), and Kyoto Encyclopedia of Genes and Genomes (KEGG) databases using DIAMOND [57] and were further compared with the Pfam database for unigene functional analysis using HMMER [58]. The number of reads aligned to each unigene in each sample was obtained using Bowtie2 v2.3.3.1 [59], and unigene expression levels (fragments per

kilobase of exon per million fragments mapped (FPKM) values [60]) were calculated using eXpress v1.5.1 [61].

The estimateSizeFactors function of the DESeq R package [62] was adopted to standardize these data, and the *p* value and fold change (FC) values of unigenes were calculated based on the nbinomTest function. Then, unigenes with a *p* value < 0.05 and an |log2FC| > 1 were defined as differentially expressed unigenes (DEGs). The GO and KEGG enrichment analyses of DEGs were performed using the ggplot2 package, and a hypergeometric distribution test was performed to calculate the significance of the enrichment of DEGs in each pathway. Hierarchical clustering of DEGs was performed, and a heatmap was used to show the expression patterns of DEGs among different samples after normalizing the row data (https://cloud.oebiotech.cn/task/detail/heatmap/, accessed on 18 September 2020). All of these DEGs were further analyzed by weighted gene coexpression network analysis (WGCNA) based on the default parameters (https://international.biocloud.net/, accessed on 7 April 2016) [63]. The interaction network of genes in each module was then visualized using Cytoscape 3.5.1 (https://cytoscape.org/, accessed on 28 September 2015).

2.5. Quantitative Real-Time Polymerase Chain Reaction (qRT-PCR) Validation

Ten DEGs involved in the flavonoid and phenylpropanoid biosynthesis, plant hormone signal transduction, starch and sucrose metabolism, and photosynthesis-related pathways were selected for qRT-PCR to verify the accuracy of the transcriptomic data. These candidate DEGs were designed with gene-specific primers based on the coding sequence (CDS) region of the obtained sequence (Table S1). Total RNA was extracted using Polysaccharides/Polyphenolics-Rich RNAprep Pure Plant Kits (Bioteke Co., Beijing, China) from the samples mentioned above according to the manufacturer's instructions, and then 1 μg of qualified RNA was reverse-transcribed to synthesize first-strand cDNA using HiScript® III RT SuperMix for qPCR (+gDNA wiper) kits (Vazyme Biotech Co., Ltd.; Nanjing, Jiangsu, China). The expression of candidate gene was detected by qRT-PCR using the ChamQTM SYBR® qPCR Master Mix Kit (Low ROX Premixed) (Vazyme Biotechnology Co., Ltd.), and the qRT-PCR was performed on an Applied Biosystems (ABI) 7500 fast real-time PCR system (ABI, Foster City, CA, USA). The PCR program included denaturing at 95 °C for 30 s, followed by 40 thermal cycle reactions of 95 °C for 10 s and 60 °C of annealing and extension for 30 s, and then melt curve analysis was performed to evaluate the specificity of the primers. *C. fortunei cyclophilin* (*CfCYP*), *actin*, and *ubiquitin-conjugating enzyme* (*CfUBC*) were used as reference genes [64], and the $2^{-\Delta\Delta ct}$ method was used to calculate the relative gene expression levels [65]. Each reaction had three biological and technical replicates. RNA-seq data and qRT-PCR data for each gene were used to calculate the normalized log2 fold change, and LA data were used as a reference. Then, linear fitting of the RNA-seq data and qRT-PCR data was performed, and the correlation index (R^2) was calculated.

2.6. Liquid Chromatography-Mass Spectrometry (LC-MS) Analysis

Needles (80 mg fresh weight) were extracted with 20 μL of 1.5 mM 2-chloro-l-phenylalanine and 1 mL of 70% methanol. The samples were milled at 60 Hz for 2 min (JXFSTPRP-24/32, Shanghai Jingxin Industrial Development Co., Ltd., Shanghai, China), sonicated at room temperature for 0.5 h (SB-5200DT, Ningbo Xinzhi Biotechnology Co., Ltd., Ningbo, Zhejiang Province, China), stored at −20 °C for 20 min, and centrifuged at 13,000 rpm at 4 °C for 10 min (TGL-16MS, Shanghai Luxiangyi Centrifuge Instrument Co., Ltd., Shanghai, China). Then, 300 μL of the supernatant were evaporated to dryness (LNG-T98, Taicang Huamei Biochemical Instrument Factory, Suzhou, Jiangsu Province, China) and reconstituted with 400 μL of 20% methanol, and the samples were recentrifuged under the conditions described above. Finally, 150 μL of the supernatant was aspirated, filtered, and transferred to an LC injection vial for LC-MS analysis.

An LC-MS system consisting of an AB ExionLC ultrahigh performance LC instrument coupled with an AB TripleTOF 6600 Plus high-resolution mass spectrometer was used to

analyze the metabolite profile. Gradient separations were performed using an ACQUITY UPLC HSS T3 column (100 mm × 2.1 mm, 1.8 µm) and a binary mobile phase consisting of 0.1% formic acid and acetonitrile aqueous solution. The acquisition of raw data and metabolomic analysis were the same as those in Zhang et al. [66].

2.7. Statistical Analysis

All data were analyzed using IBM SPSS 24.0 (Chicago, IL, USA) and are shown as the mean ± standard deviation (SD). One-way analysis of variance (ANOVA) followed by Duncan's test was used to calculate the statistical significance of differences among treatment groups, and $p < 0.05$ was considered significant. Graphs were constructed and further processed by Origin 2018 (Origin Lab, Northampton, MA, USA) and Illustrator CS6 (Adobe, San Jose, CA, USA), respectively.

3. Results

3.1. Changes in Physiological Indicators in Overwintering C. fortunei

We first investigated the physiological indicators of overwintering *C. fortunei* to explore whether its winter acclimation changed. The LT_{50} based on EL of *C. fortunei* ranged from −4.7 to −7.8 °C [2]. Compared with that of LA needles, the EL of ES needles significantly ($p < 0.05$) increased by 121.22%; H_2O_2 content and the contents of MDA, soluble sugars, and soluble proteins also increased significantly ($p < 0.05$) by 319.54%, 78.45%, 22.87%, and 30.65%, respectively (Figure 1a,c,d,g,j). However, the F_v/F_m, Y_{II}, chl content, and relative water content showed significant ($p < 0.05$) decreasing trends in overwintering *C. fortunei*, decreasing by 51.10%, 26.85%, 47.88%, and 4.91%, respectively (Figure 1b,h,k,l). In *C. fortunei* needles, SOD and POD activities did not change significantly; the soluble starch content first rose and then fell, and it dropped by 6.26% in ES needles compared with that of LA needles (Figure 1e,f,i). These results indicate that most physiological indexes change significantly in overwintering *C. fortunei*.

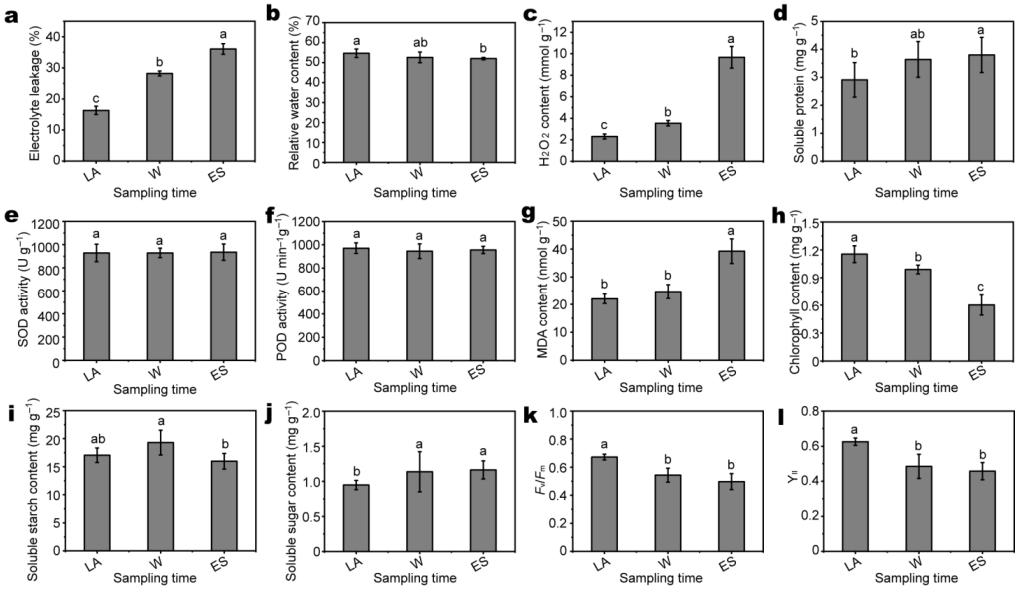


Figure 1. Physiological indicators that were determined in overwintering *Cryptomeria fortunei*. (**a**) Electrolyte leakage level; (**b**) relative water content; (**c**) hydrogen peroxide (H_2O_2) content; (**d**) soluble protein content; (**e**) superoxide dismutase (SOD) activity; (**f**) peroxidase (POD) activity; (**g**) malondialdehyde (MDA) content; (**h**) chlorophyll content; (**i**) soluble starch content; (**j**) soluble sugar content; (**k**) the maximum quantum yield of photosystem II (PSII) (*Fv/Fm*); (**l**) the effective quantum yield of PSII (Y_{II}). Sample abbreviations are as follows: ES, early spring; LA, late autumn; and W, winter. Each value in the graph is the mean ± standard deviation (n = 6), and lowercase letters above each bar indicate significant differences ($p < 0.05$).

3.2. De novo Assembly and Annotation of the C. fortunei Transcriptome

Three cDNA libraries were constructed at each different stage to comprehensively evaluate the overwintering *C. fortunei* transcriptome (Table 1). These libraries produced 460.27 M paired-end raw reads with Q30 percentages in each sample ≥ 95.36%, and 457.29 M clean reads were obtained after removing the low-quality reads and trimming the adapters. A total of 55,839 unigenes were obtained by de novo assembly (Tables S2 and S3), and the N50 and average length were 1219.86 and 1990 bp, respectively. A total of 27,769 unigenes were annotated with seven public databases (Figure S1; Tables S3 and S4). Among them, the NR database had the most annotated unigenes (27,144, 48.61%), followed by eggNOG (24,795, 44.40%), Swiss-Prot (20,620, 36.93%), and Pfam (19,817, 35.49%), while KEGG (8996, 16.11%) had the fewest annotations. We conducted a correlation analysis of each sample based on the FPKM values and observed high similarities between the three biological replicates of samples of *C. fortunei* from each period, indicating that the RNA-seq results were reliable (Figure S2).

Table 1. Sequencing parameters of the *Cryptomeria fortunei* transcriptomes from three needle samples.

Sampling Time	Sample [1]	Raw Reads (M)	Clean reads (M)	Q30 (%)	GC (%)
Late autumn (November 28)	LA_1	53.01	52.70	95.99	44.38
	LA_2	54.49	54.16	96.07	44.28
	LA_3	54.12	53.79	96.06	44.27
Winter (December 28)	W_1	52.23	51.90	95.69	44.74
	W_2	47.81	47.50	95.36	44.20
	W_3	48.82	48.49	95.60	44.26
Early spring (February 15)	ES_1	50.88	50.53	95.60	44.19
	ES_2	49.66	49.30	95.81	44.33
	ES_3	49.25	48.92	96.02	44.19

[1] ES, early spring sample; LA, late autumn sample; W, winter sample; LA_1, LA_2, and LA_3, 3 replicates of transcriptome samples.

3.3. Functional Enrichment Analysis of DEGs

The DEGs between different stages were identified to fully understand the differences in the expression levels of overwintering *C. fortunei* transcripts. A total of 16,443 DEGs, including 8270 downregulated and 10,753 upregulated DEGs, were identified (Tables S5 and S6). In the three comparisons, i.e., W vs. LA, ES vs. W, and ES vs. LA, 2567/2593, 4519/6736, and 3817/6077 down/upregulated DEGs were identified, respectively (Figure S3; Tables S7–S12).

To gain insight into the functional categories of DEGs induced by the winter condition, GO terms were used to classify the annotated down/upregulated DEGs in each comparison group. All these DEGs were divided into three categories (Figure 2). In the W vs. LA comparison, downregulated DEGs were enriched in photosynthesis- and chloroplast-related terms, such as "photosynthesis", "photosynthesis, light harvesting in photosystem I", and "chloroplast thylakoid membrane" (Figure 2a). In the ES vs. W comparison, upregulated DEGs were enriched in photosynthesis-related and "signal transduction" terms (Figure 2d); in ES vs. LA, upregulated DEGs were enriched in "signal transduction" (Figure 2f); in both comparison groups, downregulated DEGs were enriched in flavonoid biosynthetic-related processes (Figure 2c,e).

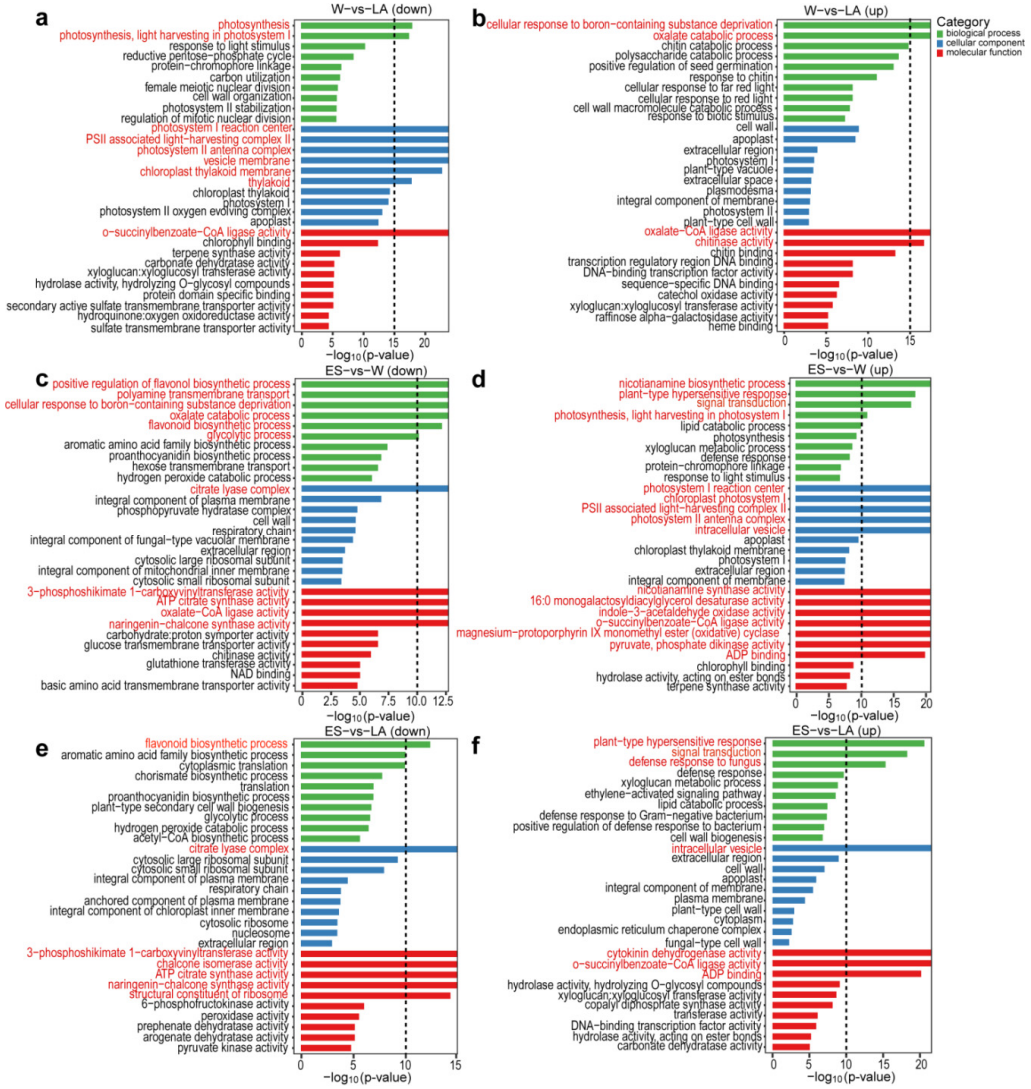


Figure 2. Gene Ontology (GO) functional annotation of differentially expressed unigenes (DEGs) in overwintering *C. fortunei*. (**a**) Downregulated DEGs in W vs. LA; (**b**) upregulated DEGs in W vs. LA; (**c**) downregulated DEGs in ES vs. W; (**d**) upregulated DEGs in ES vs. W; (**e**) downregulated DEGs in ES vs. LA; (**f**) upregulated DEGs in ES vs. LA. The *x*-axis represents $-\log_{10}(p\text{-value})$, and the *y*-axis represents the enriched GO terms. Green bars, blue bars, and red bars represent biological process terms, cellular component terms, and molecular function terms, respectively. GO terms with red text represent terms with $-\log_{10}(p\text{-value}) > 15$ or > 10. Sample abbreviations are as follows: ES, early spring; LA, late autumn; and W, winter.

The annotated DEGs for each comparison group were subjected to a KEGG enrichment analysis to determine the main overwintering acclimation-related pathways. In the W vs. LA comparison, downregulated DEGs were enriched in photosynthesis-related, "starch and sucrose metabolism" and "phenylpropanoid biosynthesis" pathways, while upregulated DEGs were enriched in "plant hormone signal transduction", carbohydrate, amino acid, and lipid metabolism, "flavonoid biosynthesis", and "phenylpropanoid biosynthesis" pathways (Figure 3a,b). In the ES vs. W comparison, downregulated DEGs were enriched in "plant hormone signal transduction", "flavonoid biosynthesis", and "phenylpropanoid biosynthesis" pathways, while upregulated DEGs were enriched in enriched in "plant hormone signal transduction", "flavonoid biosynthesis", "phenylpropanoid biosynthesis", photosynthesis-related, and "fatty acid biosynthesis" pathways (Figure 3c,d). In the ES vs. LA comparison, downregulated DEGs were enriched in "flavonoid biosynthesis" and

"phenylpropanoid biosynthesis" pathways, while upregulated DEGs were enriched in "plant hormone signal transduction", "phenylpropanoid biosynthesis", photosynthesis-related, and "fatty acid biosynthesis" pathways (Figure 3e,f). All DEGs were further subjected to a KEGG enrichment analysis. These DEGs were enriched in metabolic pathways that mainly included carbohydrate metabolism (starch and sucrose metabolism), energy metabolism (photosynthesis-related), amino acid metabolism, and lipid metabolism (fatty acid biosynthesis); these DEGs were also enriched in signal transduction pathways, including plant hormone signal transduction and MAPK signaling pathways (Figure S4). Based on these results, different metabolite synthesis processes and different signal transduction pathways are changed in overwintering *C. fortunei* needles.

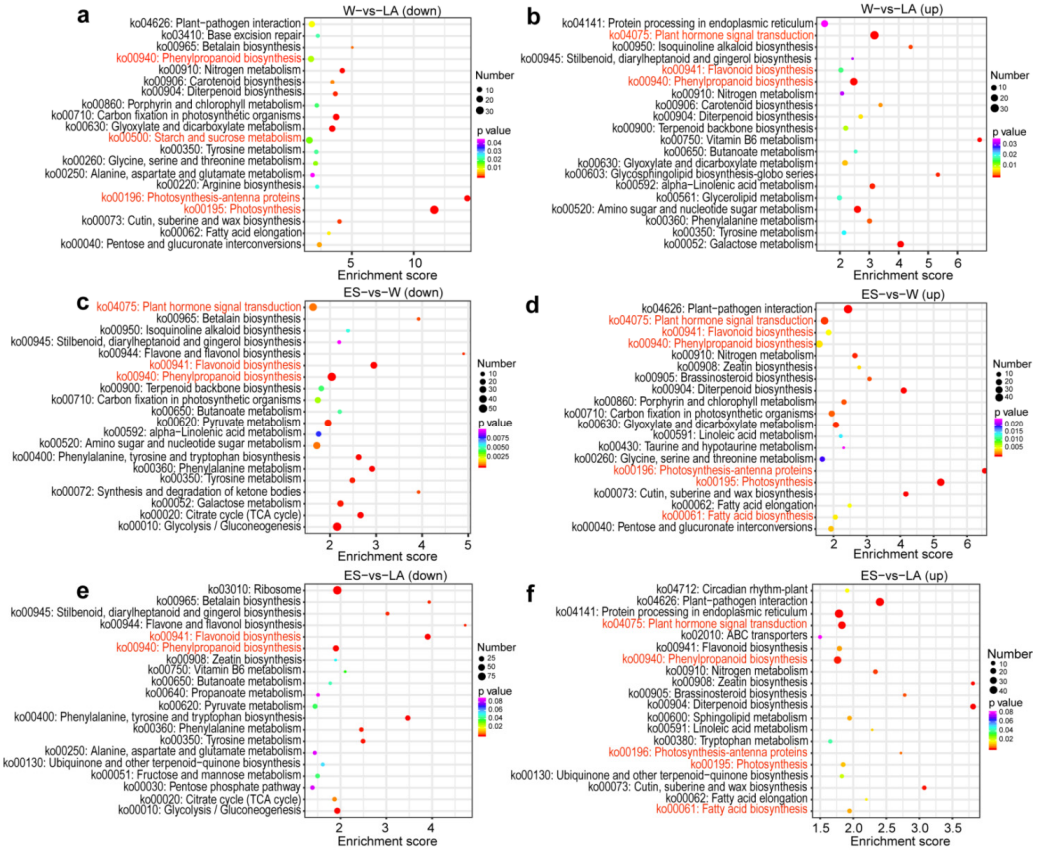


Figure 3. Kyoto Encyclopedia of Genes and Genomes (KEGG) functional annotation of DEGs in overwintering *C. fortunei*. (**a**) Downregulated DEGs in W vs. LA; (**b**) upregulated DEGs in W vs. LA; (**c**) downregulated DEGs in ES vs. W; (**d**) upregulated DEGs in ES vs. W; (**e**) downregulated DEGs in ES vs. LA; (**f**) upregulated DEGs in ES vs. LA. The *x*- and *y*-axes represent the enrichment score and enriched pathways, respectively. The size of the bubble indicates the number of associated DEGs, and the color of the bubble indicates the level of significance. Pathways indicated in red text may be related to overwintering *C. fortunei*. Sample abbreviations are as follows: ES, early spring; LA, late autumn; and W, winter.

3.4. WGCNA

WGCNA was performed to identify key genes that play a role in overwintering *C. fortunei* by filtering unigenes with low fluctuation and using an adjacency matrix weight parameter power of 19. We obtained 10 modules, and the genetic correlation between modules was small (Figure 4a), indicating that the module analysis result was reliable.

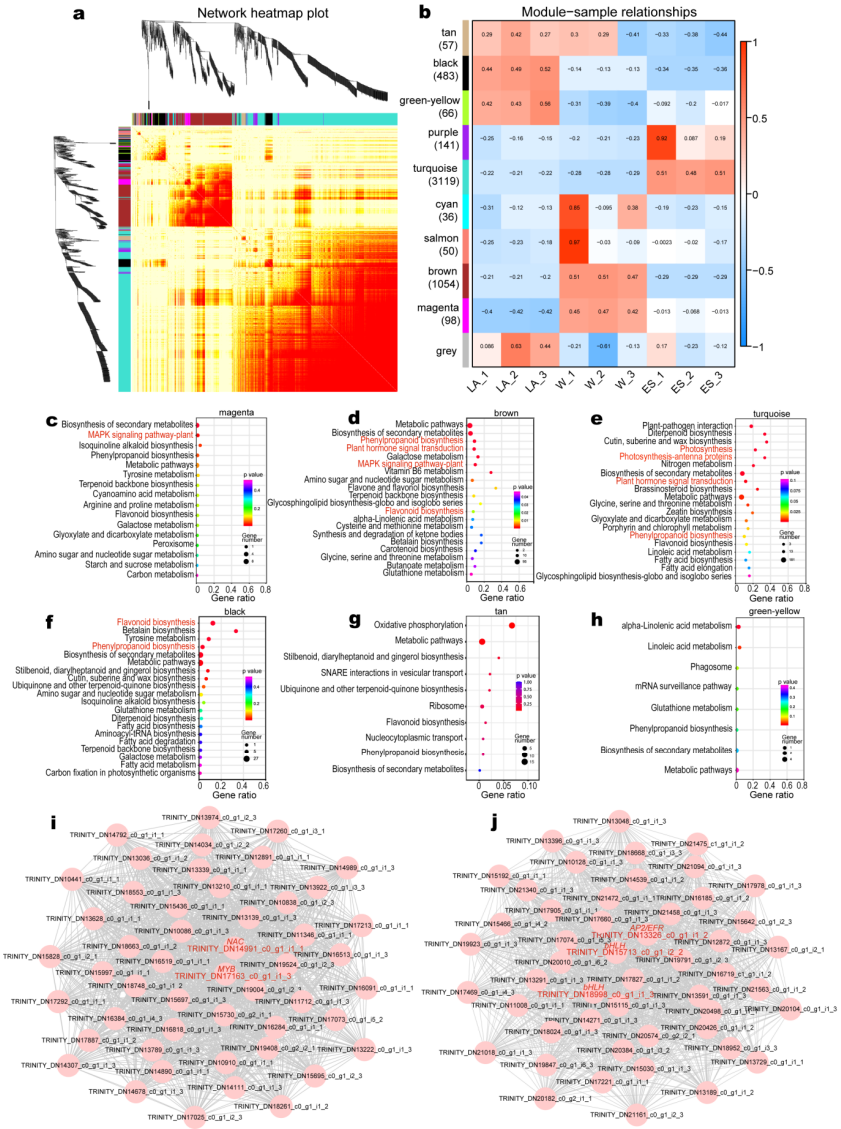


Figure 4. Construction of the DEG coexpression network and modules. (**a**) All-gene cluster heatmap. The clustering tree in the upper and left of the figure is the gene clustering tree constructed by the weighted correlation coefficient. The modules were identified by the dynamicTreeCut method. Based on a certain correlation between the gene expression levels among some modules, the corresponding modules were merged into the same module and represented by the same color. The heatmap at the bottom right is a heatmap of all gene clusters. (**b**) Module–sample relationship. The right bar represents the correlation coefficient, red/blue represents a positive/negative correlation, and numbers in the heatmap represent the correlation coefficient. Each column and each row represent each sample and module, respectively. Sample abbreviations are as follows: ES, early spring; LA, late autumn; and W, winter. LA_1, LA_2, and LA_3 represent 3 biological replicates. The text on the left is the name of each module and the number of unigenes in each module. (**c**–**h**) KEGG enrichment analysis of unigenes in the magenta (**c**), brown (**d**), turquoise (**e**), black (**f**), tan (**g**), and green-yellow (**h**) modules. The *x*- and *y*-axes represent the gene ratio and enriched pathways, respectively. The size of the bubble indicates the number of associated DEGs, and the color of the bubble indicates the level of significance. Pathways indicated in red text may be related to overwintering *C. fortunei*. (**i**) Top 50 DEGs regulatory network of *C. fortunei* in the brown module. (**j**) Top 50 DEGs regulatory network of *C. fortunei* in the turquoise module. Red text indicates hub TFs.

To further obtain the gene modules closely related to the sample period, the eigengene value of each module was analyzed in association with samples from different periods.

Nine modules containing 5104 DEGs were identified (Figure 4b); among them, the turquoise module showed the maximum number of DEGs (3119), followed by the brown module (1054) and the black module (483) (Figure 4b). The brown and magenta modules with unigenes that were correlated at high levels with W needles were associated with winter acclimation, while the turquoise module with unigenes that were correlated at high levels with ES needles was associated with the transition from dormancy to growth (Figure 4b; Figure S5). KEGG analysis was performed on the unigenes in the positively related modules (magenta, brown, and turquoise). Among them, in the magenta module, DEGs were enriched in "MAPK signaling pathway"; in the brown module, DEGs were enriched in "flavonoid biosynthesis", "MAPK signaling pathway", "plant hormone signal transduction", and "phenylpropanoid biosynthesis"; in the turquoise module, DEGs were enriched in "phenylpropanoid biosynthesis", "plant hormone signal transduction", "photosynthesis-antenna proteins", and "photosynthesis" (Figure 4c–e). The magenta module contained only five TFs including two *AP2/ERF*, two *MYB(-related)*, and one *Trihelix* (Table S13). The brown module contained a total of 41 TFs, of which *WRKY* accounted for the most, with 8, followed by *AP2/ERF*, *NAC*, *LATERAL ORGAN BOUNDARIES* (*LOB*), and *MYB* (Table S14). The turquoise module contained a total of 128 TFs, of which *AP2/ERF* accounted for the most, with 25, followed by *MYB(-related)* (16) and *bHLH* (14) (Table S15). In addition, the black, tan, and green-yellow modules containing unigenes expressed at low levels in W or ES needles were also chosen. A KEGG analysis was performed on the unigenes in each negatively correlated module, only the black module was also enriched in the "flavonoid biosynthesis" and "flavonoid biosynthesis" pathways (Figure 4f–h). Unfortunately, we detected only 13 TFs, including 7 *MYB* TFs and 3 *AP2/ERF* TFs (Table S16). We further selected the top 50 DEGs for each module (brown and turquoise) with more TFs to draw a regulatory network using Cytoscape 3.5.1 (https://cytoscape.org/, accessed on 28 September 2015). In the brown module, we identified two hub TFs (*NAC*, *TRINITY_DN14991_c0_g1_i1_1*; *MYB*, *TRINITY_DN17163_c0_g1_i1_3*); and in the turquoise module, we identified three hub TFs (*AP2/ERF*, *TRINITY_DN13326_c0_g1_i1_2*; *bHLH*, *TRINITY_DN15713_c0_g1_i2_2*, and *TRINITY_DN18998_c0_g1_i1_3*) (Figure 4i,j).

3.5. Metabolomic Analysis

We analyzed the untargeted metabolome of *C. fortunei* needles using LC-MS to investigate differences in metabolism during overwintering in *C. fortunei*. We detected a total of 15,880 metabolites in all samples, of which 9251 were annotated with determinate formulas (deposited at MetaboLights database under submission number: MTBLS3183 and MTBLS3184, Table S17). According to the compositional analysis, lipid molecules were the most abundant metabolites, accounting for 62.86% of the annotated metabolites. Our metabolomic data were reproducible, as demonstrated by cluster analysis and principal component analysis (PCA) of all metabolites, and thus could be used for subsequent analysis (Figure S6).

We obtained a total of 1320 differentially synthesized metabolites (DSMs) ($p < 0.05$) in three comparison groups (i.e., W vs. LA, ES vs. W, and ES vs. LA) (Figure S7; Table S18). In W vs. LA, 45 DSMs were significantly ($p < 0.05$) enriched in 10 metabolic pathways in four categories; among them, carbohydrate metabolism was the most enriched category, with 17 DSMs, followed by biosynthesis of other secondary metabolites (14 DSMs), amino acid metabolism (9 DSMs), and lipid metabolism (6 DSMs) (Table S19). In ES vs. W/ES vs. LA comparison, 52/45 DSMs were significantly ($p < 0.05$) enriched in 15/14 metabolic pathways in 5 categories; among them, amino acid metabolism was the most enriched category (22/23 DSMs), followed by carbohydrate metabolism (19/16 DSMs), biosynthesis of other secondary metabolites (10/12 DSMs), metabolism of cofactors and vitamins (7/4 DSMs), and lipid metabolism (3/4 DSMs) (Tables S20 and S21). Thus, overwintering *C. fortunei* needles have intense metabolic activities.

3.6. Identification of DEGs Involved in Phenylpropanoid Biosynthesis and Flavonoid Biosynthesis Pathways

The levels of genes and metabolites involved in phenylpropanoid biosynthesis and flavonoid biosynthesis pathways changed significantly ($p < 0.05$) in overwintering *C. fortunei*, according to KEGG and WGCNA analyses (Figures 3 and 4; Tables S19–S21). A total of 108 DEGs (16 genes) enriched in the phenylpropanoid biosynthesis pathway were identified. Compared with those of LA needles, 59 unigenes (54.63%) were upregulated and 46 unigenes (42.59%) were downregulated in W needles, and all these unigene expression levels in W needles increased by 21.15% (Figure 5; Table S22). Compared with those of W needles, 59 unigenes (54.63%) were upregulated and 49 unigenes (42.59%) were downregulated in ES needles, and all these unigene expression levels in ES needles decreased by 67.80% (Figure 5; Table S22). In the flavonoid biosynthesis pathway, 55 DEGs (14 genes) were identified. Compared with those of LA needles, 32 unigenes (58.18%) were upregulated and 23 unigenes (41.82%) were downregulated in W needles, and all these unigene expression levels in W needles were at high levels, increasing by 7.60% (Figure 6; Table S23). Compared with those of W needles, 20 unigenes (36.36%) were upregulated and 35 unigenes (63.64%) were downregulated in ES needles, and all these unigene expression levels in ES needles decreased by 75.81% (Figure 6; Table S23).

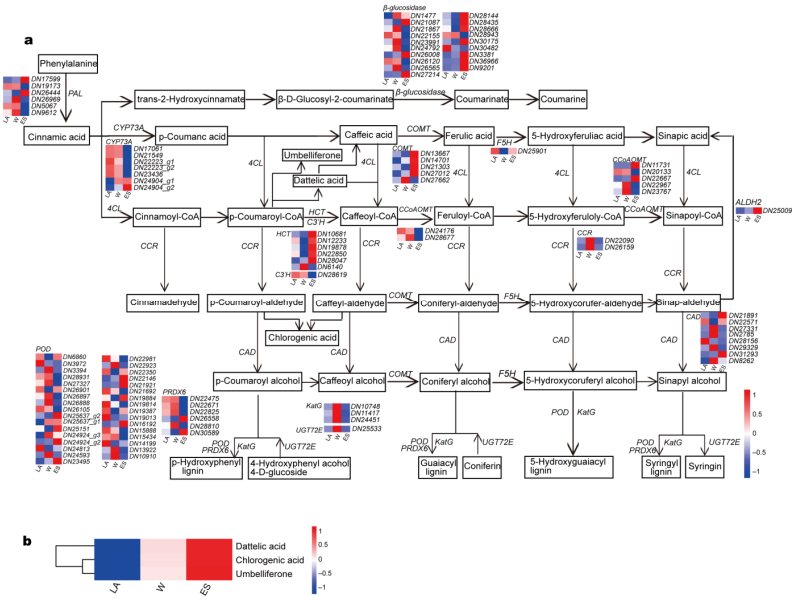


Figure 5. Metabolites and unigenes associated with phenylpropanoids that were differentially expressed in overwintering *C. fortunei*. (**a**) Unigenes involved in phenylpropanoid biosynthesis pathway. Boxed text indicates the metabolites in the metabolic pathway. Heatmap represents unigene expression levels after normalizing the row data, and red and blue represent high and low expression, respectively. Each column and each row represent a sample and a unigene, respectively. The content in italics indicates genes, and the gene abbreviations are as follows: *4CL*, *4-coumarate-CoA ligase*; *ALDH2*, *coniferyl-aldehyde dehydrogenase*; *C3'H*, *5-O-(4-coumaroyl)-D-quinate 3'-monooxygenase*; *CAD*, *cinnamyl-alcohol dehydrogenase*; *CCR*, *cinnamoyl-CoA reductase*; *CCoAOMT*, *caffeoyl-CoA O-methyltransferase*; *COMT*, *caffeic acid 3-O-methyltransferase*; *CYP73A*, *trans-cinnamate 4-monooxygenase*; *F5H*, *ferulate-5-hydroxylase*; *HCT*, *shikimate O-hydroxycinnamoyltransferase*; *KatG*, *catalase-peroxidase*; *PAL*, *phenylalanine ammonia-lyase*; *POD*, *peroxidase*; *PRDX6*, *peroxiredoxin 6*; *REF1*, *coniferyl-aldehyde dehydrogenase*; *UGT72E*, *coniferyl-alcohol glucosyltransferase*. (**b**) Hierarchical clustering heatmap of differentially synthesized metabolites (DSMs) involved in phenylpropanoid biosynthesis. Heatmap represents metabolite content after normalizing the row data. The text below the heatmap indicates the sampling time, and the text to the right of the heatmap indicates the metabolite. Sample abbreviations are as follows: ES, early spring; LA, late autumn; and W, winter.

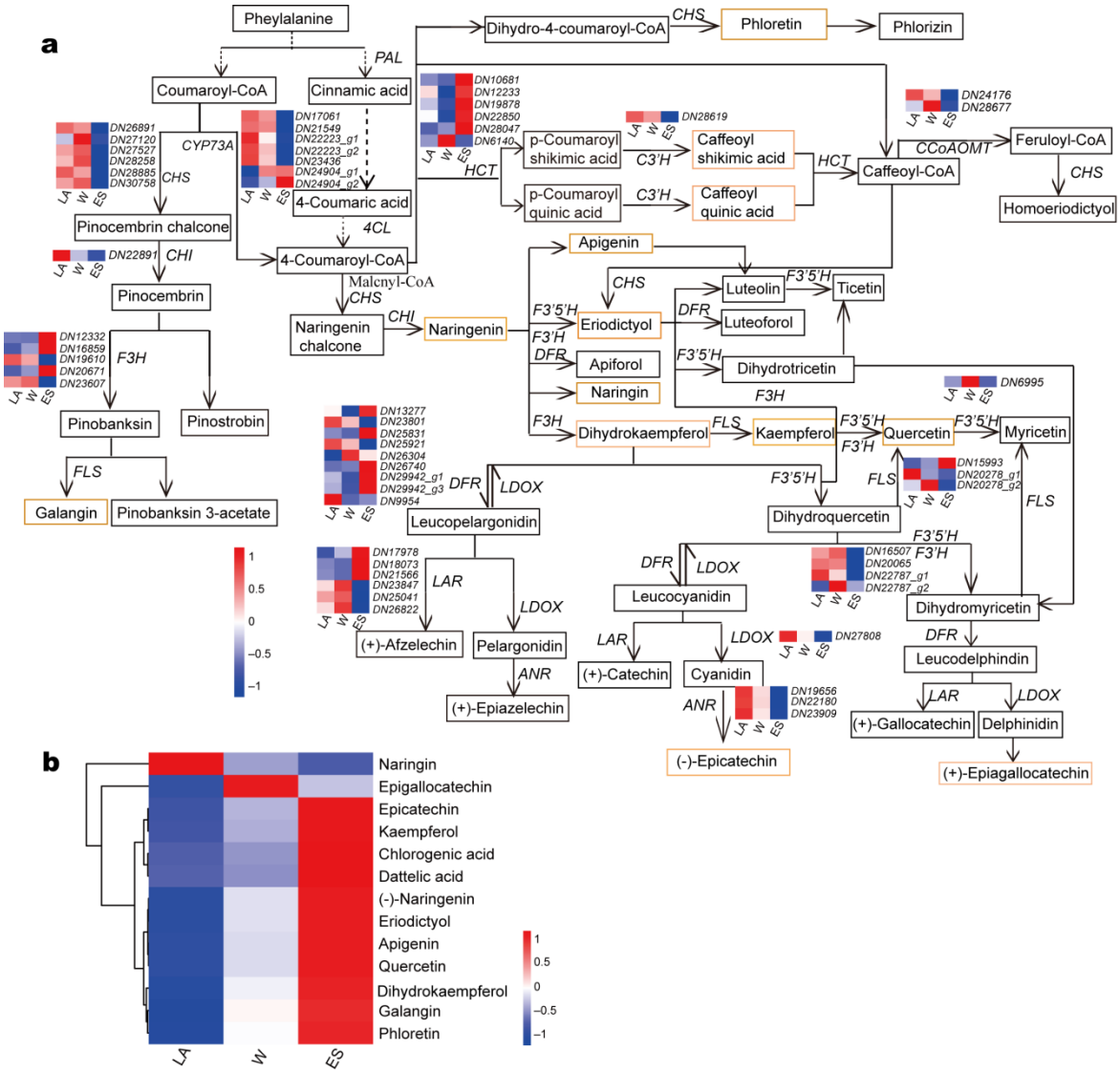


Figure 6. Metabolites and unigenes involved in flavonoid biosynthesis that were differentially expressed in overwintering *C. fortunei*. (**a**) Unigenes involved in flavonoid biosynthesis pathway. Boxed text indicates the metabolites in the metabolic pathway and text within yellow boxes indicates detected metabolites. The heatmap represents unigene expression levels after normalizing the row data, and red and blue represent high and low expression, respectively. Each column and each row represent a sample and a unigene, respectively. The content in italics indicates genes, and these gene abbreviations are as follows: *4CL*, *4-coumarate-CoA ligase*; *ANR*, *anthocyanidin reductase*; *C3'H*, *5-O-(4-coumaroyl)-D-quinate 3'-monooxygenase*; *CHI*, *chalcone isomerase*; *CHS*, *chalcone synthase*; *CCoAOMT*, *caffeoyl-CoA O-methyltransferase*; *CYP73A*, *trans-cinnamate 4-monooxygenase*; *DFR*, *bifunctional dihydroflavonol 4-reductase/flavanone 4-reductase*; *FLS*, *flavonol synthase*; *F3H*, *naringenin 3-dioxygenase*; *F3'H*, *flavonoid 3'-monooxygenase*; *F3'5'H*, *flavonoid 3',5'-hydroxylase*; *HCT*, *shikimate O-hydroxycinnamoyltransferase*; *LAR*, *leucoanthocyanidin reductase*; *LDOX*, *leucoanthocyanidin dioxygenase*; *PAL*, *phenylalanine ammonia-lyase.* (**b**) Hierarchical clustering heatmap of DSMs involved in flavonoid biosynthesis. Heatmap represents metabolite content after normalizing the row data. The text below the heatmap indicates the sampling time, and the text to the right of the heatmap indicates the metabolite. Red represents high metabolite contents, and blue represents low metabolite contents. Sample abbreviations are as follows: ES, early spring; LA, late autumn; and W, winter.

We subsequently used LC-MS data from *C. fortunei* needles at the abovementioned three stages to investigate the corresponding metabolic changes in overwintering *C. for-*

tunei. In the phenylpropanoid biosynthesis and flavonoid biosynthesis pathways—except epigallocatechin, which was most abundant in W needles, and naringin—which was most abundant in LA needles, the other metabolites showed an upward trend during the overwintering process, with the highest abundance in ES needles (Figures 5b and 6b). These results suggest phenylpropanoid biosynthesis and flavonoid biosynthesis may play an important role in overwintering *C. fortunei*.

3.7. Identification of DEGs Involved in Plant Hormone Signal Transduction Pathways

The expression of genes involved in plant hormone signal transduction pathways was significantly ($p < 0.05$) altered in overwintering *C. fortunei*, as verified by KEGG enrichment analyses and WGCNA of the DEGs (Figures 3 and 4). Plant hormone signal transduction pathways include eight major hormone (i.e., auxin/indole-3-acetic acid (IAA), cytokinin (CTK), gibberellin (GA), ABA, ethylene, brassinosteroid (BR), jasmonic acid (JA), and salicylic acid (SA)) pathways.

In the ABA, ethylene, JA, and BR signal transduction pathways, most downstream DEGs were highly expressed in W needles (Figure 7; Table S24). Specifically, 18 DEGs were related to ABA biosynthesis; among them, four downstream *ABA responsive element binding factors* (*ABFs*) and one positively regulated *serine/threonine-protein kinase* (*SnRK2s*)) had the highest expression levels in W needles. Nine DEGs were related to JA biosynthesis, and two downstream *myelocytomatosis cooncogene homolog 2* (*MYC2*) unigenes and two positively regulated DEGs (one *JA-amino synthetase* (*JAR1)* and one coding *ronatine-insensitive protein 1* (*COI-1*) unigene) were upregulated in W needles. Eight DEGs related to ethylene signal transduction were identified; one downstream unigene coding *EIN3-binding F-box protein* (*EBF1_2*) and one positively regulated *mitogen-activated protein kinase 6* (*MPK6*) had the highest expression in W needles, while four negatively regulated DEGs (3 *ethylene receptors* (*ETRs*) and one *serine/threonine-protein kinase* (*CTR1*)) were expressed at low levels in W needles. In addition, eight downstream DEGs (one *cyclin D3* (*CYCD3*) and seven *touch-inducible gene* (*TCH4s*)) were involved in the BR pathway, and among them, four *TCH4*s peaked in W needles.

In the IAA, CTK, GA, and SA signal transduction pathways, most downstream DEGs were highly expressed in ES needles (Figure 6; Table S10). We observed 23 DEGs in the IAA pathway, 13 downstream DEGs (12 *small-auxin-up-RNA* (*SAUR*), and one *growth hormone response* (*GH3*)*-like* unigene) were upregulated in ES needles. Ten DEGs related to GA biosynthesis (one encoding *Asp-Glu-Leu-Leu-Ala* (*DELLA*) protein, five *GA-insensitive dwarf2* (*GID2*) unigenes, three *GA-insensitive dwarf1* (*GID1*) unigenes, and *phytochrome-interacting factor 4* (*PIF4*) unigene) were identified. The downstream *PIF4* and three positively regulated *GID2s* were the most highly expressed in ES needles, while one negatively regulated *GID1* was expressed at low levels in ES needles. Six DEGs were related to SA biosynthesis, including two *pathogenesis-related genes* (*PR-1s*), two *TGACG motif-binding factors* (*TGAs*), and two *nonexpressor of PR-1s* (*NPR1s*). Among them, the downstream gene *PR-1* and positively regulated *TGA* showed upward expression trends, reaching a peak in ES needles. Eight positively regulated DEGs (two *histidine-containing phosphotransfer* proteins (*AHPs*), two *CER1s*, one *two-component response regulator ARR-A family* (*A-ARR*), and three *two-component response regulator ARR-B* family members (*ARR-Bs*)) involved in the CTK pathway were highly expressed in ES needles.

We found 13 DSMs upstream of each hormone signal transduction pathway (Figure 7). Among them, in the upstream of IAA, CTK, GA, and SA signal transduction pathways, eight DSMs had the highest contents in ES needles. Specifically, except L-tryptophan which increased first and then decreased slightly and GA A5 which decreased first and then increased, the other metabolite contents increased and had the highest contents in ES needles (Figure 7). In the upstream of ethylene and ABA signal transduction pathways, we only detected three DSMs. Based on these results, the activated hormone signal transduction pathway may play a regulatory role in overwintering *C. fortunei*.

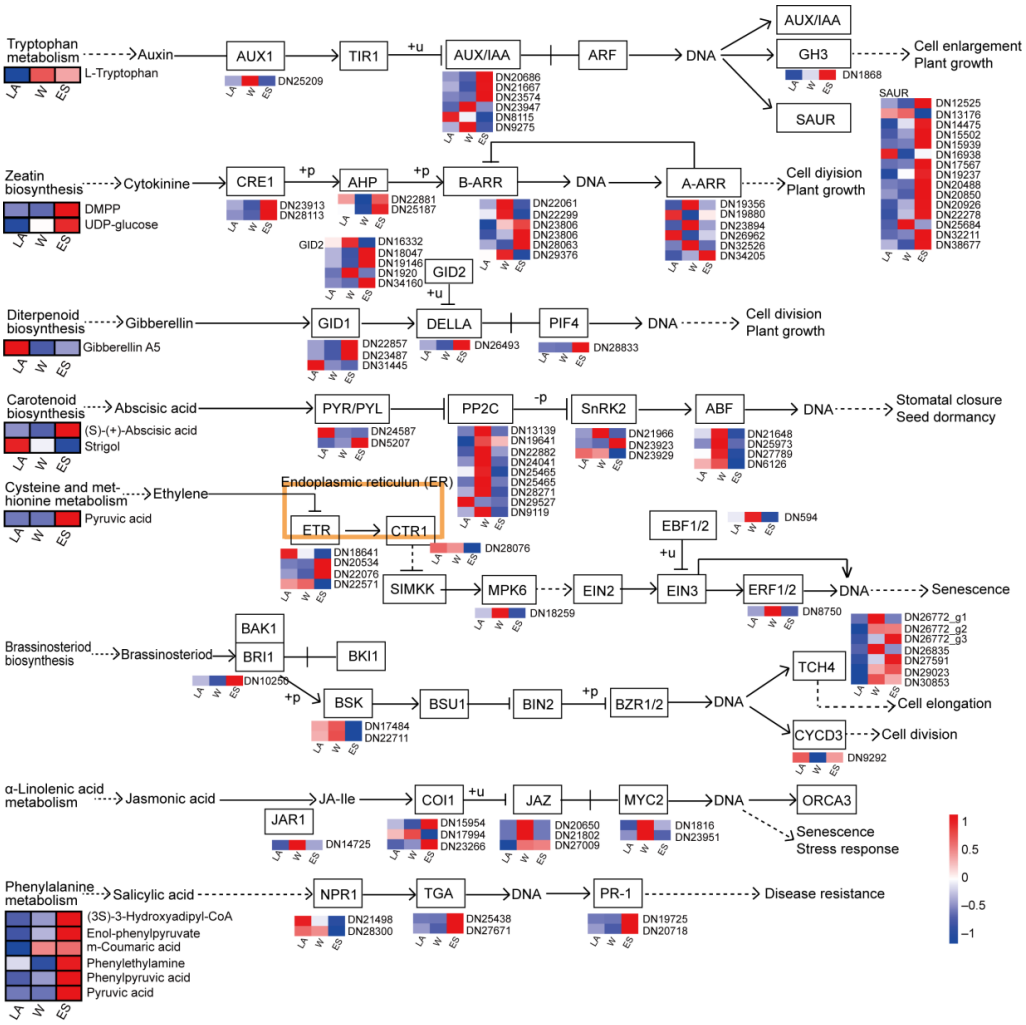


Figure 7. Plant hormone signal transduction-related genes that were differentially expressed in overwintering *C. fortunei*. Normal arrows indicate promotion, and T-shaped arrows indicate inhibition. The brown box indicates endoplasmic reticulum (ER). After normalizing the row data, boxed heatmaps indicate the metabolite contents, and unframed heatmaps represent unigene expression levels. Red represents highly expressed unigenes/high metabolite contents, and blue represents unigenes with low expression/low metabolite content. The text below the heatmap indicates the sampling time (ES, early spring; LA, late autumn; and W, winter). Gene abbreviations are as follows: *A-ARR, two-component response regulator ARR-A family; ABF, ABA responsive element binding factor; AHP, histidine-containing phosphotransfer protein; AUX1, auxin influx carrier; AUX/IAA, auxin-responsive protein IAA; ARF, auxin response factor; BAK1, brassinosteroid insensitive 1-associated receptor kinase 1; B-ARR, two-component response regulator ARR-B family; BKI1, BIN2, brassinosteroid insensitive 2; BRI1 kinase inhibitor 1; BRI1, brassinosteroid insensitive 1; BSK, BR-signaling kinase; BSU1, serine/threonine-protein phosphatase BSU1; BZR1_2, brassinosteroid resistant 1/2; CTR1, serine/threonine-protein kinase; COI-1, coronatine-insensitive protein 1; CYCD3, cyclin D3; DELLA, Asp-Glu-Leu-Leu-Ala protein; EBF1_2, EIN3-binding F-box protein; EIN2, ethylene-insensitive protein 2; ERF1, ethylene-responsive transcription factor 1; ETR, ethylene receptor; GH3, growth hormone response; GID1,* gibberellin-*insensitive dwarf1; GID2, F-box protein GID2; JAR1, jasmonic acid-amino synthetase; JAZ, jasmonate ZIM domain-containing protein; MPK6, mitogen-activated protein kinase 6; MYC2, myelocytomatosis oncogene homolog 2; NPR1, nonexpressor of PR-1; ORCA2_3, AP2/ERF-domain transcription factor; PIF4, phytochrome-interacting factor 4; PP2C, protein phosphatase 2C; PR1, pathogenesis-related protein 1; PYR/PYL, pyrabactin resistance/pyr1-like; SIMKK, mitogen-activated protein kinase kinase 4/5; SnRK2, serine/threonine-protein kinase SRK2; SAUR, small-auxin-up-RNA; TCH4; touch-inducible gene; TGA, TGACG Motif-binding factor; TIR1, transport inhibitor response 1.*

3.8. Identification of DEGs Involved in Starch and Sucrose Metabolism and Photosynthesis-Related Pathways

We found that 100 annotated DEGs (28 genes) were significantly ($p < 0.05$) enriched in the starch and sucrose metabolism pathway (Figure S8; Table S25). Compared with those of LA needles, 58 unigenes (58.00%) were upregulated and 41 unigenes (41.00%) were downregulated in W needles, and all these unigene expression levels in W needles increased by 29.19%; compared with those of W needles, 48 unigenes (48.00%) were upregulated and 52 unigenes (52.00%) were downregulated in ES needles, and all these unigene expression levels in ES needles decreased by 23.36% (Figure S8; Table S25). Correspondingly, the contents of three DSMs in this pathway also increased and had the highest levels in ES needles (Table S26).

In addition, we identified many DEGs that were enriched in the "photosynthesis" and "photosynthesis-antenna proteins" categories. Forty-three DEGs encoding photosystem I (PSI), PSII, photosynthetic electron transport, cytochrome b6/f complex, and F-type ATPase were identified (Figure S9a; Table S27). These DEGs were downregulated in W needles and then peaked in ES needles (Figure S9a; Table S27). Similarly, 18 DEGs related to the synthesis of light-harvesting complexes (LHC) I and II were found to be involved in photosynthesis-antenna proteins (Figure S9b; Table S28). Except for *LHC I chl a/b binding protein 5* (*LHCA5*), which showed a decreasing trend, the other genes were downregulated first in W needles and then upregulated in ES needles (Figure S9b; Table S28). Therefore, we speculate that starch and sucrose metabolism and photosynthesis-related pathways might also be important in overwintering *C. fortunei*.

3.9. Identification of DEGs Involved in (Unsaturated) Fatty Acid Biosynthesis or Related to LT-Related Proteins

We identified 25 and 6 DEGs in the fatty acid and unsaturated fatty acid biosynthesis pathways, respectively (Tables S29 and S30). In the fatty acid pathway, all these unigene expression levels increased and had the highest expression in ES needles; meanwhile, in the unsaturated fatty acid biosynthesis pathway, all these unigene expression levels increased first and then decreased, and they had the highest expression in W needles (Tables S29 and S30). In particular, two desaturases, i.e., *FAB2* and *FAD2*, were upregulated in W needles. In addition, we found that two DSMs in the fatty acid biosynthesis pathway, among them, the content of Hexanoyl-CoA was > 100-fold that of 3-Ketohexanoyl-CoA, and it exhibited the highest content in ES needles (Table S31).

In addition, we detected 44 LT-related DEGs (Table S32). Among them, *DREB*s, LEA and *glycerol-3-phosphate acyltransferase* (*GPAT6*) were significantly upregulated in overwintering *C. fortunei*, with the highest expression observed in ES needles. Thirteen LTPs were upregulated first and then downregulated, with the highest expression in W needles. Thus, genes involved in (unsaturated) fatty acid biosynthesis pathways or related to LT-related proteins may be important in overwintering *C. fortunei*.

3.10. Verification of RNA-seq Results Using qRT-PCR

We performed qRT-PCR to analyze the transcriptional abundance of 10 selected DEGs to verify the accuracy of the RNA-seq data (Figure 8). The expression profiles of these DEGs obtained using qRT-PCR were very similar to the RNA-seq data ($R^2 = 0.8137$, Figure 8k), confirming the reliability of the RNA-seq data, which potentially reflects actual changes in overwintering *C. fortunei*.

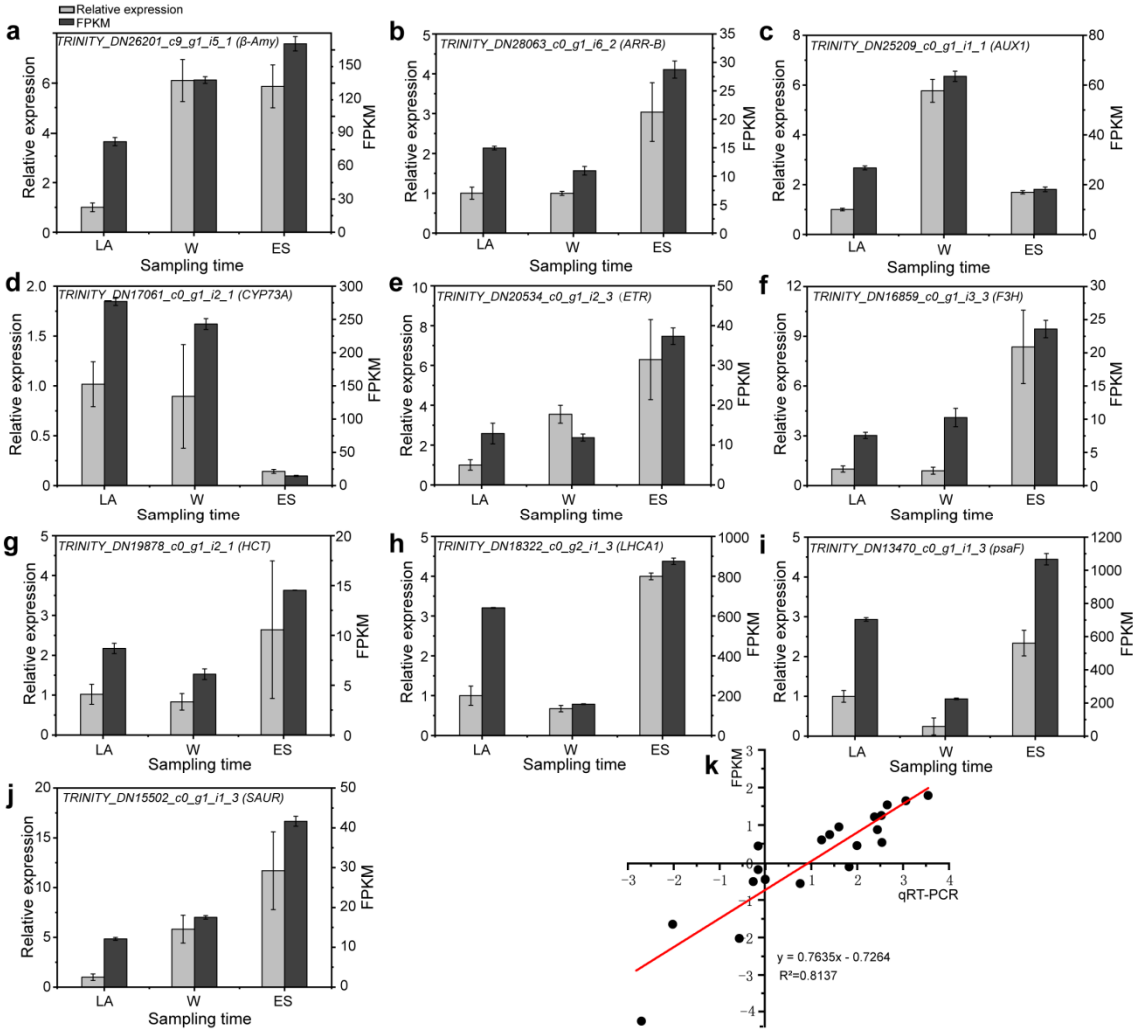


Figure 8. Expression of *C. fortunei* genes in response to cold winters as determined by quantitative real-time polymerase chain reaction (qRT-PCR). Differentially expressed unigenes involved in starch and sucrose metabolism (**a**), flavonoid/phenylpropanoid biosynthesis (**d**,**f**,**g**), plant hormone signal transduction (**b**,**c**,**e**,**j**), and photosynthesis-related (**h**,**i**) pathways. The *x*-axis represents samples (i.e., ES, early spring; LA, late autumn; and W, winter), the *y*-axis represents FPKM or unigene relative expression level, and each value is the mean ± standard deviation (n = 3). FPKM, fragments per kilobase of exon per million fragments mapped. Gene abbreviations are as follows: *β-Amy, beta-amylase; ARR-B, two-component response regulator ARR-B family; AUX1, auxin influx carrier; CYP73A, trans-cinnamate 4-monooxygenase; ETR, ethylene receptor; F3H, naringenin 3-dioxygenase; HCT, shikimate O-hydroxycinnamoyltransferase; LHCA1, light-harvesting complex I chlorophyll a/b binding protein 1; psaF, photosystem I subunit III; SAUR, small-auxin-up-RNA.* (**k**) Linear fitting of qRT-PCR data and FPKM data were performed after normalizing their row data with LA data as a reference, respectively. The *x*-axis represents qRT-PCR data, and the *y*-axis represents FPKM data.

4. Discussion

4.1. Changes in Physiological Indicators in Overwintering C. fortunei

We found that during the overwintering process, the EL level, MDA content, and H_2O_2 content of *C. fortunei* needles increased (Figure 1a,c,g). Membrane permeability is an important physiological indicator for evaluating plant stress, and EL is inversely proportional to plant resistance; that is, the higher the EL level is, the more severe the damage caused by stress [67,68]. MDA, the final product of lipid peroxidation, and H_2O_2 content are oxidative burst signals that stimulate the production of ROS. Increases in the contents of these two factors reflect an increase in plant stress [67,69]. These indicators

showed that the overwintering process of *C. fortunei* damaged its needles, leading to excessive ROS accumulation in the needles, which subsequently increased the peroxidation of plant membrane lipids and damaged the mesophyll cell membrane. Interesting, these indicators peaked in ES needles, we believe this may be caused by the fact that the actual temperature sampled at the ES period is lower than the actual temperature sampled at the W period.

Relative water content showed a decreasing trend as overwintering progressed (Figure 1b). Plants exposed to LT stress usually show symptoms of water stress due to cold-induced inhibition of water uptake and loss [70,71]. However, the change in the relative water content was small; we think it was related to dry weather (Tables S33 and S34), but on the other hand, it may be related to the species specificity of *C. fortunei*. In addition, various osmotic substances that play an important role in osmotic adjustment, as soluble protein, soluble starch, and soluble sugar contents accumulated rapidly in W needles and then slowly increased or decreased in ES needles (Figure 1d,i,j; Table S26); consistently, unigenes associated with soluble sugar metabolism were upregulated in W needles (Figure S8; Tables S25 and S35), and sugars such as raffinose play an important protective role in cold acclimation of conifers. We suspect that adjustments in the levels of these osmotic substances in W needles increase the concentration of cell fluid, reduce the osmotic potential, and increase the ability of cells to absorb or retain water, thereby enhancing winter acclimation; while in ES needles, the change of osmotic substances was beneficial to the transition from dormant to growing period of *C. fortunei*.

4.2. Changes in Photosynthesis in Overwintering *C. fortunei*

Chl content showed a decreasing trend as overwintering progressed (Figure 1h). A decrease in chl contents often indicates stress-induced leaf damage [72], and for the evergreen plant *C. fortunei*, the decrease in resistance will directly lead to the premature degradation of chl and result in tawny *C. fortunei* needles. F_v/F_m and Y_{II} significantly ($p < 0.05$) decreased in W needles and then was at the low levels (Figure 1k,l). F_v/F_m reflects the potential maximum photosynthetic capacity of the plant, and the decrease in F_v/F_m reveals photochemical inhibition of PSII. The decrease might be attributed to the increased levels of light-harvesting antennas, which induce nonradiative quenching of excited energy, leading to irreversible activation of non-photochemical quenching (NPQ) [3]. When the PSII function is impaired in winter, the contents of lutein and pigments in the lutein cycle may increase to cause a partial loss of chl and the reduction in the epoxidation of the lutein cycle pool, resulting in the aggregation of light-harvesting antennae, allowing PSII photochemistry to safely dissipate absorbed light into heat when strongly inhibited [73,74]. The winter reorganization of the coniferous daylighting device maintains a large amount of chl in a quenched and photoprotected state [74]. Therefore, we speculate that the normal metabolism and photosynthetic function of needles decrease in W needles.

It is evident that the transcriptome of overwintering *C. fortunei* underwent significant changes in photosynthesis. For example, GO and KEGG analyses showed that in the W vs. LA comparison, downregulated DEGs were enriched in photosynthesis- and chloroplast-related terms (Figures 2a and 3a), while in ES vs. W, upregulated DEGs were enriched in photosynthesis- and chloroplast-related terms (Figures 2d and 3d). Photosynthesis, which occurs on the chloroplast, refers to the process by which green plants absorb light energy, convert CO_2 and H_2O into energy ATP, and release O_2. Chloroplast is composed of outer and inner membranes, stroma, and thylakoid. Four major protein complexes, i.e., PSI and LHCA, PSII and LHCB, cytochrome b6-f complex, and F-type H+-ATPase, involved in electron transfer in light reactions, are mostly ordered mosaic in the thylakoid membrane [75]. These protein complexes work together to capture external light energy, split H_2O, release O_2, promote electron transfer and transport, and reduce ATP, and finally complete photosynthesis [76,77]. In this study, we obtained 43 DEGs related to photosynthesis (Figure S9a; Table S27). Among them, PSII, PSI, photosynthetic electron transport, cytochrome b6/f complex, and ATPase genes were downregulated in W needles

and then upregulated in ES needles (Figure S9a; Table S27). This indicates that in W needles, protein synthesis of PSII and PSI and the functional structure of thylakoids are blocked, resulting in the lack of photosynthetic pigments and the decline in photosynthesis. In ES needles, DEGs related to the photosynthesis were upregulated, indicating that the photosynthetic inhibition phenomenon of *C. fortunei* needles was alleviated at the ES period. In this study, we obtained 18 DEGs related to photosynthesis–antenna proteins, and the *LHC* gene family showed an obvious trend of first decreasing and then increasing (Figure S9a; Table S27). In photosynthesis, the LHC pigment–protein complex can capture light energy and absorb, transmit, and transform it by PSII and PSI [78,79]. At the W period, the reduction of *LHC gene* in the needles indicates that the pigment protein complexes that capture light energy are reduced, and the needle photosynthesis is reduced (Table S28), while at the ES period, the needle photosynthesis is enhanced. Therefore, we speculate that at the W period, the normal metabolism and photosynthetic function of the *C. fortunei* needles were significantly reduced, while needle photosynthesis improves at the ES period, which is beneficial to the transition from the dormant period to the growth period.

4.3. Genes Involved in the Flavonoid and Phenylpropanoid Biosynthesis Pathways Are Activated to Promote Metabolite Accumulation in Overwintering C. fortunei

The flavonoid and phenylpropanoid biosynthesis pathways are important plant secondary metabolism pathways. Simple or complex phenolic compounds are mainly considered to be antioxidants derived through the phenylpropanoid biosynthesis pathway, and these substances play an important role in the plant response to adversity [80,81]. Here, in the phenylpropanoid biosynthesis pathway, we found that most genes were upregulated in W needles (Figure 5a; Table S22); we also detected the accumulation of metabolites in overwintering *C. fortunei,* and metabolite contents were at the highest level in ES needles (Figure 5b). We believe that genes regulate metabolites and that changes in gene expression levels precede the changes in metabolite contents. From LA to W period, the upregulated gene expression was beneficial to the accumulation of metabolites in W needles; at the W period, the gene expression levels peaked and continued to promote the accumulation of metabolites. These results were similar to the results of studies in sweet cherries (*Prunus avium*) [82] and *C. fortunei* [83]. Specifically, enhancing the expression of genes in the phenylpropanoid biosynthesis pathway promotes enzymatic activity of phenylpropanoid biosynthesis enzymes, thereby increasing the accumulation of phenylpropanoid substances [82–84].

In plant tissues or organs, flavonoid accumulation protects plants from metal stress, radiation damage, and nutrient deficiency and enhances abiotic stress resistance [85,86]. We found that most metabolite contents were upregulated and at the highest levels in ES needles (Figure 6b), which is consistent with the deepest yellowish-brown phenotype of *C. fortunei* needles in February. We found that the expression of genes was downregulated during the overwintering process, but the expression levels in the W needles were similar to those in LA needles; at the ES period, the gene expression level was very low, but the metabolite contents reached the maximum values (Figure 6; Table S23). Metabolites are likely to be an accumulation process, and increased expression levels of flavonoid biosynthesis pathway genes lead to more flavonoid accumulation [87,88]. At the W period, high expression of genes continued to promote the accumulation of metabolites. Therefore, metabolite contents exceed those in the W period and are at the highest level in ES needles. In addition, *C. fortunei* needles may be affected by a variety of factors under natural conditions; except for this pathway genes, flavonoid biosynthesis is regulated by TFs, resulting in extremely complex flavonoid biosynthesis regulatory network, but further research is needed.

In general, in the phenylpropanoid and flavonoid biosynthesis pathways, the high expression genes of W needles promote the synthesis of metabolites, resulting in a continued increase in DSM contents in ES needles (> those in W needles) and enhancing the stress

resistance in winter. Meanwhile, the low expression of genes in ES needles facilitates its transition from dormant to growth stage.

4.4. Overwintering C. fortunei Plants Form a Complex Hormone Signaling Network

Although plants contain very small amounts of hormones, as secondary signals, hormones can trigger a series of signal cascade reactions and ultimately induce stress response genes [89], which play a vital role in the stress physiology of plants. The expression levels of genes in the plant hormone signal transduction pathways exhibited significant changes in overwintering *C. fortunei* (Figure 7). We further divided these plant hormone signal transduction pathways into two categories (i.e., ABA, JA, BR, and ethylene; IAA, CTK, GA, and SA) according to their downstream gene expression profiles.

The most researched plant hormone signal transduction pathway is the ABA-dependent pathway. ABA is considered to be an essential messenger for plants to adapt to abiotic stress, and it plays a key role in activating the plant LT response through its (in)dependent pathways [12,90]. The endogenous ABA level increases rapidly, quickly closing stomata to reduce water loss [91] and increasing the content of osmotic adjustment substances to cope with environmental pressure, which in turn activates specific signaling pathways and changes gene expression [92]. Downstream *ABF* was upregulated in W needles (Figure 7; Table S24). Expression levels of *PtrABF* from trifoliate orange (*Poncirus trifoliata*) were induced by treatments with dehydration, low temperature, and ABA [93]. Therefore, ABA-mediated signals may enhance the regulation of the winter acclimation of *C. fortunei*. JA and ethylene are also key factors controlling the plant abiotic stress response [94–96]. Studies have shown that exposure to LT stress leads to increased endogenous levels of these hormones [97,98]. In our study, key enzymes (such as *MYC2, JAR1, COI-1, MPK6,* and *EBF1_2*) in the JA or ethylene biosynthesis pathway were upregulated in W needles (Figure 7; Table S24). BRs can improve cold stress tolerance with fewer trade-offs in terms of growth [99]. Correspondingly, we found *TCH4* was expressed at the highest level in W needles (Table S24). *TCH4* is upregulated in BR regulation, enhancing its response to environmental stimuli [100]. In general, the abovementioned four hormone metabolism pathways were generally upregulated in W needles, which may inhibit growth and development, thereby improving winter acclimation (Figure 9).

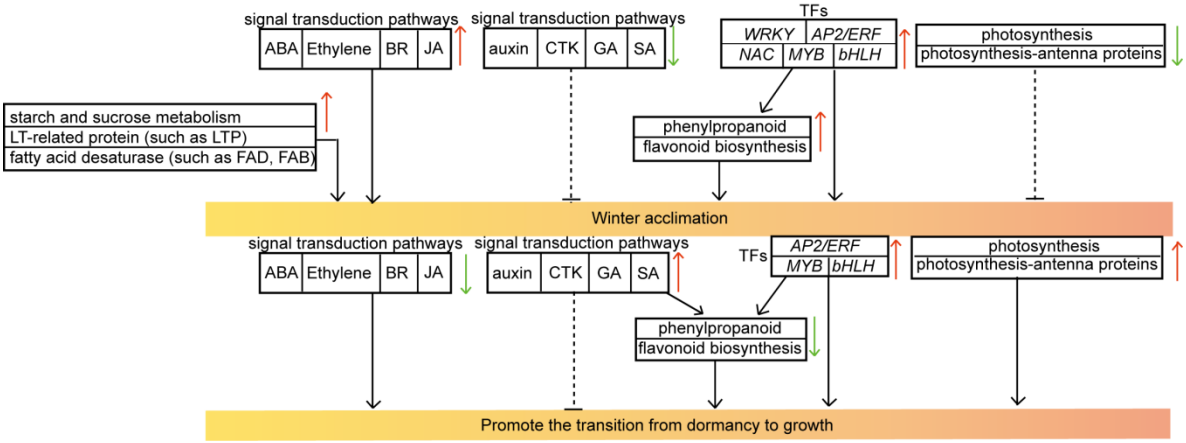


Figure 9. Regulatory network and mechanism of overwintering *C. fortunei*. Green arrows indicate downregulated expression; red arrows indicate upregulated expression. Black arrows indicate facilitation of winter acclimation or the transition from dormancy to growth, and dashed arrows indicate inhibition of winter acclimation or the transition from dormancy to growth. The abbreviations are as follows: ABA, abscisic acid; *AP2/ERF, apetala2/ethylene-responsive factor*; *bHLH, basic helix-loop-helix*; CTK, cytokinin; GA, gibberellin; JA, jasmonic acid; *MYB, v-myb avian myeloblastosis viral oncogene homolog*; *NAC, NAM, ATAF1/2, and CUC2*; SA, salicylic acid.

Other hormones may also affect plant responses to cold winter stress. The effect of growth-related GA hormones on abiotic stress is becoming clearer. Four DEGs (three *GID2*s and one downstream gene *PIF4)* peaked in ES needles, while one *GID1* was expressed at low levels in ES needles (Figure 7; Table S24). GA binds to its receptor GID1 protein, recognizes the DELLA protein in the nucleus, forms the GA-*GID1-DELLA* complex, and induces the conformational change of the GRAS domain of the DELLA protein, thereby allowing VHIID and LHRII motifs of DELLA to recognize the F-box protein GID2/SLY1 [101–103]. At the same time, the SCFSLY1-*GID2* complex in turn promotes the polyubiquitination of the DELLA protein, which is then degraded by the 26S proteasome, thereby responding to GA and eliminating its inhibitory effect on plant growth [101,104,105]. Therefore, most *GID2*s in the GA signal transduction pathway peaked in ES needles (Figure 7), eliminating the inhibition of plant growth, and upregulated *PIF4* further promoted a new round of the plant growth cycle at the ES period [106]. In addition, most IAA-related (*SAUR* and *GH3*), SA-related (*PR-1 and TGA*), and CTK-related (*AHP, A-ARR, CER1 and ARR-B*) downstream DEGs were also upregulated in ES needles (Figure 7; Table S24). These metabolic pathways were also related to plant growth, which was generally inhibited at the W stage, leading to a decrease in the associated content; at the ES stage, these metabolic pathways may promote the plant to end dormancy and enter the dormancy–growth transition period. In summary, plant hormone signal transduction pathways exert a strong stimulatory effect on overwintering *C. fortunei*; therefore, we propose a regulatory mechanism for overwintering *C. fortunei* (Figure 9).

4.5. Fatty Acid Desaturase and LT-Related Proteins Are Activated to Promote Winter Acclimation in Overwintering C. fortunei

We found that *FAB2* and *FAD2* were upregulated in W needles (Table S30). LT induced the accumulation of unsaturated fatty acids, and these fatty acid desaturases are divided into three types, i.e., fatty acyl ACP desaturases, fatty acyl CoA desaturases, and fatty acyl lipid desaturases. *FAD2* and *FAB2* encode stearoyl-ACP desaturases. *FAD2* is located downstream of the oleic acid synthesis pathway. It catalyzes the formation of double bonds at the 12th carbon atom of the fatty acid chain, and controls the synthesis and contents of oleic acid, linoleic acid, and other various unsaturated fatty acids [107]. *FAB2* is an upstream gene that regulates oleic acid synthesis. It adds a double bond between C9 and C10 of the long chain of 18-carbon fatty acids. After converting stearoyl-ACP to oleoyl ACP, the body uses the acetyl-CoA transport pathway to transport oleoyl-ACP to the endoplasmic reticulum to synthesize oleic acid, which determines the content of oleic acid in plants [108]. We speculate that the high expression of fatty acid desaturase promotes the synthesis and increases the contents of oleic acid, linoleic acid, and other unsaturated fatty acids during winter cold acclimation, improving LT tolerance.

We found that *GPAT* and LEA were upregulated and expressed at the highest levels in ES needles (Table S30). As the first enzyme in the glycerolipid synthesis pathway, *GPAT* converts the fatty acyl group at the sn-1 position into 3-phosphoglycerol to synthesize 1-acyl-S-glycero-3-phosphate. After being catalyzed by acyl fatty acid desaturase, 1-acyl-S-glycero-3-phosphate continues to be desaturated to increase the level of cis-unsaturated fatty acids in phosphatidylglycerol. High *GPAT* expression may improve cold resistance in plants [45,109]. LEA proteins improve plant tolerance to cold and freezing stress [13,110]. Phytohydrin, also known as LEA protein, is highly hydrophilic and has low complexity [111]; it is presumed to function as a molecular chaperone that prevents protein aggregation under cold stress [112]. Therefore, we propose that the expression of LEA improves LT tolerance. For example, heterologous expression of *CsLEA1* from camellia confers cold stress tolerance to *Escherichia coli* and yeast [113]. However, *GPAT* and LEA were at the highest levels in ES needles; we think it may be caused by the lower temperature when we sampled in ES than in W. In addition, LTPs were upregulated first and then downregulated, with the highest expression observed in W needles (Table S32). With the decrease in temperature, the fluidity of plant cell membrane decreases. LTP is involved in lipid transfer

between biofilms in biological cells. When plants encounter LT stress, LTP functions as a regulatory protein to stabilize plasma membrane activity; therefore, high levels of LTP better regulate the fluidity of the cell membrane to reduce LT damage [114].

4.6. TFs Show Upregulated Expression in Response to Cold Winters

We found that *WRKY*, *AP2/ERF*, *NAC*, *MYB*, and *LOB* were highly expressed in W needles (Figure S5; Table S36). These TFs participate in many processes of plant growth and development and are widely involved in the plant response to abiotic stress [15,17,19,21,115,116]. For example, these TFs play an active role in regulating the accumulation of phenylpropane and flavonoids [117–121]; therefore, we speculated that these TFs were upregulated in W needles, which promoted related gene expression, causing the accumulation of these metabolites. *DREB/CBF* in *AP2/ERF* plays a key role in regulating the LT response [25], and *ICE-CBF* is a key regulatory pathway for coping with LT stress [24,122]; LT induces Ca^{2+} signaling to activate the DREB/CBF pathway and other TFs such as *MYB* and *NAC*, inducing the expression of various cold-responsive (*COR*) genes (Table S32); *WRKY*s are activated by the *mitogen-activated protein kinase* (*MAPK*) cascade and upregulate the *COR* gene through a mechanism independent of *CBF* [123,124]. The plant specific *LOB domain* (*LBD*) gene family encodes transcriptional regulators that function in organ development [125]; however, further research remains to be seen to determine whether *LOB* plays a role in winter stress of *C. fortunei*. In addition, compared with that of LA needles, we also found nine *bHLH* were highly expressed in W needles (Table S36). *ICE1* encodes the *MYC*-like *bHLH* TF, which can bind to the *MYC* recognition element in the *CBF3* promoter and induce *CBF3* expression during LT acclimation [126]. Therefore, we further suspect that these highly expressed TFs play an active role in the accumulation of metabolites involved in the flavonoid biosynthesis and phenylpropanoid biosynthesis pathways and winter acclimation.

Notably, we also found that *AP2/ERF*, *MYB*, and *bHLH* were upregulated in ES needles (Figure S5; Tables S5 and S37). These TFs play an important regulatory role in plant development [127–129]. For example, *GAMYB*s are a kind of *MYB*-like TF induced by GA, which are key genes in the GA signaling pathway. Their increased expressions promote the gene expressions in the GA signaling pathway, thereby promoting the breaking of plant dormancy [130]; *bHLH* TFs regulate plant growth by interacting with *auxin-responsive factors* (*ARFs*) [131]. Some *AP2/ERF*s can be rapidly induced to express, while some *AP2/ERF*s respond slowly, indicating that there may be two response modes, i.e., dependent and independent of hormone signaling pathways [132]; in addition, previous studies have demonstrated that *AP2/ERF*s are widely involved in the regulation of plant hormone-mediated responses such as ABA, ethylene, GA, CTK, and BR [133–135], thus the regulation is complex and specific *AP2/ERF*s may play different roles at different growth stages. In general, we infer that these TFs play a positive regulatory role in the transition from dormancy to growth. However, the regulatory roles of specific TFs remain to be further studied.

4.7. Comparison with Extremely and Moderately Cold-tolerant Plant Species

Extremely cold-tolerant Chinese wild *Vitis* species (*Vitis amurensis*) can safely withstand temperatures as low as −40 °C [136]. When the leaves responded to 0 °C cold stress for 48 h, leaf swelling, wilting, and chlorosis (leaf yellowing) were observed, but not on a large scale; starch grain volume increased, and obvious voids appeared in the chloroplast, indicating that the leaves were slightly damaged by cold stress [137]. Similarly, this cold stress-induced symptom was also seen in the cold-sensitive plant *Saintpaulia*, where cell death was also found in limited areas of leaves [138]. During cold stress, the induction mechanism of programmed cell death (PCD) is thought to differ between cold-tolerant and sensitive plant species: cold-tolerant plants respond by initiating the hardening process rather than PCD, while cold-sensitive species cause the entire plant to die fairly quickly [2,139].

Siberian spruce (*Picea obovata*) survives extreme temperatures, typically −20 to −40 °C. At low winter temperatures (−10 to −35 °C), increased glycolipid abundance, changes

in fatty acid desaturation and lipid composition, and the accumulation of proteins with possible cryoprotective functions (such as LEA) were observed [6,7,43]. According to these results, the extremely frost-tolerant tree species have similar responses to LT as the moderately hardy species investigated in the present study, suggesting that the plants have a fundamental and conservative adaptation to LT stress. In addition, we also observed changes in the genes/metabolites of plant hormone signal network responses, photosynthesis and phenylpropanoid and flavonoid biosynthesis (Tables S19–S24), which is similar to many LT studies [134,140]. For example, plant hormone signaling network responses and photosynthesis were also observed in poplar exposed to brief (16 h) LT stress at 4 °C [141]; *Hosta ventricosa* increases genistein and rutin levels by activating phenylpropanoid biosynthesis and flavonoid biosynthesis pathways to protect against LT injury [140]. Further analyses of whether other plant species with extreme or moderate cold tolerance have similar trends in metabolic synthesis and gene expression levels under LT stress in relatively mild winter environments are necessary.

Cold tolerance is a genetically complex trait regulated by complex gene, metabolic, and protein regulatory networks [142,143]. A large number of specific response genes, metabolites, or proteins highlight the regulatory mechanisms associated with cold stress [142,144,145]. For example, Pang et al. [146] identified upregulated genes of cold-treated Catawba rhododendron (*Rhododendron catawbiense*) seedlings using transcriptome sequencing, and genes such as *FAD*, delta 1-pyrroline-5-carboxylate synthetase (*P5CS*), *LEA* gene, antioxidant enzyme CAT/SOD gene, *SnRK2*, *AP2/ERF,* and *WRKY*, were thought to play important roles in cold stress. Angelcheva et al. [43] analyzed the DSMs of Siberian spruce needles under natural conditions with sufficient LT exercise and before antifreeze exercise, and found that carbohydrates, amino acids, polyamines, and lipid metabolism-related metabolites may play an important role in rapid adaptation to extreme LTs. Kjellsen et al. [44] identified 43 proteins including dehydrin, HSP70, cyclophilin, rich glycine protein, and several ROS intermediate scavenging proteins of Siberian spruce during natural antifreeze exercise, which accumulated in response to LT stress. In addition, metabolites or proteins are regulated by genes [144,147]. Overall, cold signals are sensed by cell membrane receptors and transduced by calcium and *MAPK*, leading to the activation of stress-sensitive genes; genes further activate the expression of downstream cold-responsive genes to synthesize protective enzymes, metabolites, and proteins to reconstitute energy, metabolites, proteins, and a new homeostasis of redox balance, thereby enhancing tolerance to cold stress [137,148].

5. Conclusions

In this study, physiological, metabolomic, and transcriptomic analyses of overwintering *C. fortunei* were performed. *C. fortunei* experienced increased levels of stress as overwintering progressed based on physiological data. DEGs and DSMs involved in photosynthesis, carbohydrate metabolism, lipid metabolism, and plant hormone signal transduction-related pathways were identified, and we propose a regulatory mechanism of overwintering *C. fortunei.* Upregulated signal transduction pathways (ABA, ethylene, BR, and JA), phenylpropanoid and flavonoid biosynthesis, starch and sucrose metabolism, LT-related protein, fatty acid desaturase, downregulated signal transduction pathways (GA, SA, CTK, and IAA), and photosynthesis-related pathways promote the winter acclimation of *C. fortunei*, while the opposite expression pattern in ES needles promotes its transition from dormancy to growth. TFs *WRKY*, *NAC*, *AP2/ERF*, *bHLH*, and *MYB* enhance winter acclimation, whereas *AP2/ERF*, *MYB,* and *bHLH* enhance the transition from dormancy to growth. These results provide valuable information for the genetic improvement of winter acclimation and for further research on other winter-adaptation mechanisms in plants.

Supplementary Materials: The following supporting information can be downloaded at: https://www.mdpi.com/article/10.3390/f13081249/s1, Figure S1: annotation information obtained from seven different databases; Figure S2: chart showing the results of the quality assessment chart of transcriptome samples; Figure S3: Venn diagram of differentially expressed unigenes (DEGs) in overwintering *C. fortunei*; Figure S4: Kyoto Encyclopedia of Genes and Genomes (KEGG) functional

annotations of DEGs in overwintering *C. fortunei*; Figure S5: hierarchical clustering heatmap of unigenes; Figure S6: quality control chart of metabolome samples; Figure S7: venn diagrams of differentially synthesized metabolites (DSMs); Figure S8: unigenes in the starch and sucrose metabolism pathways that were differentially expressed in overwintering *C. fortunei*; Figure S9: unigenes in photosynthesis-related metabolism pathways that were differentially expressed in overwintering *C. fortunei*; Table S1: all primers for unigenes used in this study; Table S2: sequences for all unigenes; Table S3: annotation for all unigenes; Table S4: annotation statistics of *C. fortunei* unigenes; Table S5: all downregulated DEGs; Table S6: all upregulated DEGs; Table S7: downregulated DEGs in W vs. LA; Table S8: upregulated DEGs in W vs. LA; Table S9: downregulated DEGs in ES vs. W; Table S10: upregulated DEGs in ES vs. W; Table S11: downregulated DEGs in ES vs. LA; Table S12: upregulated DEGs in ES vs. LA; Table S13: transcription factors (TFs) in the magenta module; Table S14: TFs in the brown module; Table S15: TFs in the turquoise module; Table S16: TFs in the black, tan, and green-yellow modules; Table S17: all detected metabolites; Table S18: all DSMs; Table S19: KEGG analysis of DSMs in W vs. LA; Table S20: KEGG analysis of DSMs in ES vs. W; Table S21: KEGG analysis of DSMs in ES vs. LA; Table S22: DEGs in the phenylpropanoid biosynthesis pathway; Table S23: DEGs in the flavonoid biosynthesis pathway; Table S24: DEGs associated with plant hormone signal transduction; Table S25: DEGs involved in starch and sucrose metabolism; Table S26: DSMs associated with starch and sucrose metabolism; Table S27: DEGs involved in photosynthesis; Table S28. DEGs in photosynthesis–antenna proteins; Table S29: DEGs involved in fatty acid biosynthesis; Table S30: DEGs involved in the biosynthesis of unsaturated fatty acids; Table S31: DSMs in fatty acid biosynthesis; Table S32: low temperature-related DEGs; Table S33: Climate data in Nanjing from November 2019 to February 2020; Table S34: Climate data in Nanjing from 2000 to 2020; Table S35: *trehalose 6-phosphate synthase/phosphatase (TPS)* expression; Table S36: differentially expressed TFs in W vs. LA; Table S37: differentially expressed TFs in ES vs. W.

Author Contributions: Conceptualization, J.X. (Jin Xu); formal analysis, Y.Z., H.H., J.Y. and J.X. (Jinyu Xue); data curation, Y.Z.; writing—original draft, Y.Z.; writing—review and editing, Y.Z. and J.X. (Jin Xu); supervision, J.X. (Jin Xu); funding acquisition, J.X. (Jin Xu); project administration, J.X. (Jin Xu). All authors have read and agreed to the published version of the manuscript.

Funding: This research was funded by grants from the Fujian Province Science and Technology Research Funding for the Fourth Tree Breeding Program of Chinese fir (Min Lin Ke 2016-35), Seed Industry Innovation and Industrialization Project of Fujian Province (ZYCX-LY-202101), Postgraduate Research & Practice Innovation Program of Jiangsu Province (KYCX21_0918), and Priority Academic Program Development of Jiangsu Higher Education Institutions (PAPD).

Institutional Review Board Statement: Not applicable.

Informed Consent Statement: Not applicable.

Data Availability Statement: The raw read data that support the findings of this study are available in the NCBI BioProject database (accession numbers: PRJNA697258 (SAMN17672899—901, SAMN17672905—907, and SAMN17672911—913)). The climate data set is provided by National Tibetan Plateau Data Center (http://data.tpdc.ac.cn, accessed on 1 June 2022).

Acknowledgments: We would like to give thanks to Jinhui Chen for her experimental help in determining chlorophyll fluorescence parameters.

Conflicts of Interest: The authors declare no conflict of interest.

References

1. Fu, L.; Yu, Y.; Robert, R.M. Taxodiaceae. In *Flora of China*; Wu, Z., Peter, H.R., Eds.; Science Press: Beijing, China, 1999; Volume 4, pp. 54–64.
2. Zhang, Y.; Zhu, Q.; Zhang, M.; Guo, Z.; Yang, J.; Mo, J.; Cui, J.; Hu, H.; Xu, J. Individual *Cryptomeria fortunei* hooibrenk clones show varying degrees of chilling stress resistance. *Forests* **2020**, *11*, 189. [CrossRef]
3. Han, Q.; Shinohara, K.; Kakubari, Y.; Mukai, Y. Photoprotective role of rhodoxanthin during cold acclimation in *Cryptomeria japonica*. *Plant Cell Environ.* **2003**, *26*, 715–723. [CrossRef]
4. Chinnusamy, V.; Zhu, J.; Zhu, J.K. Cold stress regulation of gene expression in plants. *Trends Plant Sci.* **2007**, *12*, 444–451. [CrossRef] [PubMed]

5. Strimbeck, G.R.; Schaberg, P.G. Going to extremes: Low-temperature tolerance and acclimation in temperate and boreal conifers. In *Plant Cold Hardiness: From the Laboratory to the Field*; Gusta, L.V., Wisniewski, M., Tanino, K.K., Eds.; CABI: Oxfordshire, UK, 2009; pp. 226–239.
6. Strimbeck, G.R.; Schaberg, P.G.; Fossdal, C.G.; Schroder, W.P.; Kjellsen, T.D. Extreme low temperature tolerance in woody plants. *Front. Plant Sci.* **2015**, *6*, 884. [CrossRef] [PubMed]
7. Kjellsen, T.D.; Yakovlev, I.A.; Fossdal, C.G.; Strimbeck, G.R. Dehydrin accumulation and extreme low-temperature tolerance in Siberian spruce (*Picea obovata*). *Tree Physiol.* **2013**, *33*, 1354–1366. [CrossRef] [PubMed]
8. Strimbeck, G.R.; Kjellsent, T.D.; Schaberg, P.G.; Murakami, P.F. Cold in the common garden: Comparative tolerance of boreal and temperate conifer foliage. *Trees* **2007**, *21*, 557–567. [CrossRef]
9. DeHayes, D.H.; Schaberg, P.G.; Strimbeck, G.R. Red spruce (*Picea rubens* Sarg.) cold hardiness and freezing injury susceptibility. In *Conifer Cold Hardiness*; Bigras, F.J., Colombo, S.J., Eds.; Springer: Dordrecht, The Netherlands, 2001; Volume 1, pp. 495–529.
10. Bleecker, A.B.; Kende, H. Ethylene: A gaseous signal molecule in plants. *Annu. Rev. Cell Dev. Biol.* **2000**, *16*, 1–18. [CrossRef]
11. Greer, D.; Berry, J.; Björkman, O. Photoinhibition of photosynthesis in intact bean leaves: Role of light and temperature, and requirement for chloroplast-protein synthesis during recovery. *Planta* **1986**, *168*, 253–260.
12. Ishitani, M. Genetic analysis of osmotic and cold stress signal transduction in *Arabidopsis*: Interactions and convergence of abscisic acid-dependent and abscisic acid-independent pathways. *Plant Cell* **1997**, *9*, 1935–1949.
13. Thomashow, M.F. Plant cold acclimation: Freezing tolerance genes and regulatory mechanisms. *Annu. Rev. Plant Physiol. Plant Mol. Biol.* **1999**, *50*, 571–599. [CrossRef]
14. Zhang, Y.; Zhang, M.; Hu, H.; Yang, J.; Cui, J.; Xu, J. Cloning and cold-resistance analyses of *CfICE1* gene in *Cryptomeria fortunei*. *Plant Physiol. Biochem.* **2021**, *162*, 456–467. [CrossRef] [PubMed]
15. Chen, L.; Yu, S.; Li, S.; Zhang, L.; Zou, C.; Yu, D. The role of *WRKY* transcription factors in plant abiotic stresses. *BBA-Gene Regul. Mech.* **2012**, *1819*, 120–128. [CrossRef] [PubMed]
16. de Souza, R.R.; Rouhana, L.V.; Sadeque, A.; Koga, L.; Clough, S.J.; Calla, B.; de Oliveira Paiva, P.D.; Korban, S.S. Genome-wide expression of low temperature response genes in *Rosa hybrida* L. *Plant Physiol. Biochem.* **2020**, *146*, 238–248.
17. Ruan, M.B.; Guo, X.; Wang, B.; Yang, Y.L.; Li, W.Q.; Yu, X.L.; Zhang, P.; Peng, M. Genome-wide characterization and expression analysis enables identification of abiotic stress-responsive *MYB* transcription factors in cassava (*Manihot esculenta*). *J. Exp. Bot.* **2017**, *68*, 3657–3672. [CrossRef]
18. Wang, L.; Xiang, L.; Hong, J.; Xie, Z.; Li, B. Genome-wide analysis of *bHLH* transcription factor family reveals their involvement in biotic and abiotic stress responses in wheat (*Triticum aestivum* L.). *3 Biotech* **2019**, *9*, 236. [CrossRef] [PubMed]
19. An, J.P.; Li, R.; Qu, F.J.; You, C.X.; Wang, X.F.; Hao, Y.J. An apple *NAC* transcription factor negatively regulates cold tolerance via *CBF*-dependent pathway. *J. Plant Physiol.* **2017**, *221*, 74–80. [CrossRef]
20. Li, Y.; Li, L.; Ding, W.; Li, H.; Shi, T.; Yang, X.; Wang, L.; Yue, Y. Genome-wide identification of *Osmanthus fragrans bHLH* transcription factors and their expression analysis in response to abiotic stress. *Environ. Exp. Bot.* **2020**, *172*, 103990. [CrossRef]
21. Mizoi, J.; Shinozaki, K.; Yamaguchi-Shinozaki, K. *AP2/ERF* family transcription factors in plant abiotic stress responses. *BBA-Gene Regul. Mech.* **2012**, *1819*, 86–96. [CrossRef]
22. Zhou, L.; Rajesh, Y.; Jin, L.; Cao, H. Genome-wide identification and expression analysis of *MYB* gene family in oil palm (*Elaeis guineensis* Jacq.) under abiotic stress conditions. *Environ. Exp. Bot.* **2020**, *180*, 104245. [CrossRef]
23. Akhtar, M.; Jaiswal, A.; Taj, G.; Jaiswal, J.P.; Qureshi, M.I.; Singh, N.K. *DREB1/CBF* transcription factors: Their structure, function and role in abiotic stress tolerance in plants. *J. Genet.* **2012**, *91*, 385–395. [CrossRef]
24. Kim, Y.S.; Lee, M.; Lee, J.H.; Lee, H.J.; Park, C.M. The unified *ICE–CBF* pathway provides a transcriptional feedback control of freezing tolerance during cold acclimation in *Arabidopsis*. *Plant Mol. Biol.* **2015**, *89*, 187–201. [CrossRef] [PubMed]
25. Thomashow, M.F. Molecular basis of plant cold acclimation: Insights gained from studying the *CBF* cold response pathway. *Plant Physiol.* **2010**, *154*, 571–577. [CrossRef] [PubMed]
26. Agarwal, P.K.; Jha, B. Transcription factors in plants and ABA dependent and independent abiotic stress signalling. *Biol. Plant.* **2010**, *54*, 201–212. [CrossRef]
27. Huang, X.; Shi, H.; Hu, Z.; Ao, L.; Erick, A.; Chen, L.; Fu, J. ABA is involved in regulation of cold stress response in bermudagrass. *Front. Plant Sci.* **2017**, *8*, 1613. [CrossRef]
28. Hormaetxe, K.; Hernandez, A.; Becerril, J.M.; García-Plazaola, J.I. Role of red carotenoids in photoprotection during winter acclimation in *Buxus sempervirens* leaves. *Plant Biol.* **2004**, *6*, 325–332. [CrossRef]
29. Hughes, N.M. Winter leaf reddening in "evergreen" species. *New Phytol.* **2011**, *190*, 573–581. [CrossRef]
30. Hormaetxe, K.; Becerril, J.M.; Hernandez, A.; Esteban, R.; García-Plazaola, J.I. Plasticity of photoprotective mechanisms of *Buxus sempervirens* L. leaves in response to extreme temperatures. *Plant Biol.* **2007**, *9*, 59–68. [CrossRef]
31. Tanaka, A. Photosynthetic activity in winter needles of the evergreen tree *Taxus cuspidata* at low temperatures. *Tree Physiol.* **2007**, *27*, 641–648. [CrossRef]
32. Oquist, G.; Huner, N.P. Photosynthesis of overwintering evergreen plants. *Annu. Rev. Plant Biol.* **2003**, *54*, 329–355. [CrossRef]
33. Hughes, N.M.; Burkey, K.O.; Lavender-Bares, J.; Smith, W.K. Xanthophyll cycle pigment and antioxidant profiles of winter-red (anthocyanic) and winter-green (acyanic) angiosperm evergreen species. *J. Exp. Bot.* **2012**, *63*, 1895–1905. [CrossRef]
34. Fischer, B.B.; Hideg, E.; Krieger-Liszkay, A. Production, detection, and signaling of singlet oxygen in photosynthetic organisms. *Antioxid. Redox Signal.* **2013**, *18*, 2145–2162. [CrossRef] [PubMed]

35. Ruelland, E.; Vaultier, M.; Zachowslci, A.; Hurry, V. Cold signalling and cold acclimation in plants. *Adv. Bot. Res.* **2009**, *49*, 35–150.
36. Nozzolillo, C.; Isabelle, P.; Das, G. Seasonal changes in the phenolic constituents of jack pine seedlings (*Pinus banksiana*) in relation to the purpling phenomenon. *Can. J. Bot.* **1990**, *68*, 2010–2017. [CrossRef]
37. Morozova, O.; Hirst, M.; Marra, M.A. Applications of new sequencing technologies for transcriptome analysis. *Annu. Rev. Genom. Hum. Genet.* **2009**, *10*, 135–151. [CrossRef] [PubMed]
38. Kong, X.M.; Zhou, Q.; Luo, F.; Wei, B.D.; Wang, Y.J.; Sun, H.J.; Zhao, Y.B.; Ji, S.J. Transcriptome analysis of harvested bell peppers (*Capsicum annuum* L.) in response to cold stress. *Plant Physiol. Biochem.* **2019**, *139*, 314–324. [CrossRef]
39. Yael, K.; Adi, D.F.; Doron, H.; Ron, P. Effects of harvest time on chilling tolerance and the transcriptome of 'Wonderful' pomegranate fruit. *Postharvest Biol. Tec.* **2019**, *147*, 10–19.
40. Wang, F.; Chen, S.; Cai, K.; Lu, Z.; Yang, Y.; Tigabu, M.; Zhao, X. Transcriptome sequencing and gene expression profiling of *Pinus sibirica* under different cold stresses. *Breed Sci.* **2021**, *71*, 550–563. [CrossRef]
41. Wang, F.; Chen, S.; Liang, D.; Qu, G.; Chen, S.; Zhao, X. Transcriptomic analyses of *Pinus koraiensis* under different cold stresses. *BMC Genom.* **2020**, *21*, 10. [CrossRef]
42. Vergara, A.; Haas, J.C.; Aro, T.; Stachula, P.; Street, N.R.; Hurry, V. Norway spruce deploys tissue-specific responses during acclimation to cold. *Plant Cell Environ.* **2022**, *45*, 427–445. [CrossRef]
43. Angelcheva, L.; Mishra, Y.; Antti, H.; Kjellsen, T.D.; Funk, C.; Strimbeck, R.G.; Schroder, W.P. Metabolomic analysis of extreme freezing tolerance in Siberian spruce (*Picea obovata*). *New Phytol.* **2014**, *204*, 545–555. [CrossRef]
44. Kjellsen, T.D.; Shiryaeva, L.; Schröder, W.P.; Strimbeck, G.R. Proteomics of extreme freezing tolerance in Siberian spruce (*Picea obovata*). *J. Proteom.* **2010**, *73*, 965–975. [CrossRef] [PubMed]
45. Nishida, I.; Murata, N. Chilling sensitivity in plants and cyanobacterta: The crucial contribution of membrane lipids. *Annu. Rev. Plant Physiol. Plant Mol. Biol.* **1996**, *47*, 541–568. [CrossRef] [PubMed]
46. Zhang, Y.; Yang, J.; Zhu, L.; Xue, J.; Hu, H.; Cui, J.; Xu, J. Identification of microRNAs and their target genes related to needle discoloration of evergreen tree Chinese cedar (*Cryptomeria fortunei*) in cold winters. *Planta* **2021**, *254*, 31. [CrossRef] [PubMed]
47. Tsarouhas, V.; Kenney, W.A.; Zsuffa, L. Application of two electrical methods for the rapid assessment of freezing resistance in *Salix eriocephala*. *Biomass Bioenerg.* **2000**, *19*, 165–175. [CrossRef]
48. Li, H.S.; Sun, Q.; Zhao, S.J.; Zhang, W.H. *Principles and Techniques of Plant Physiology and Biochemistry Experiments*, 1st ed.; Higher Education Press: Beijing, China, 2000; pp. 164–261.
49. Lichtenthaler, H.K.; Wellburn, A.R. Determinations of total carotenoids and chlorophylls a and b of leaf extracts in different solvents. *Analysis* **1983**, *11*, 591–592. [CrossRef]
50. Maxwell, N.; Johnson, G.N. Chlorophyll fluorescence-a practical guide. *J. Exp. Bot.* **2000**, *51*, 659–668. [CrossRef]
51. Draper, H.H.; Hadley, M. Malondialdehyde determination as index of lipid peroxidation. *Method. Enzymol.* **1990**, *186*, 421–431.
52. Bradford, M.M. A rapid and sensitive method for the quantitation of microgram quantities of protein utilizing the principle of protein-dye binding. *Anal. Biochem.* **1976**, *72*, 248–254. [CrossRef]
53. Britton, C.; Maehly, A.C. Assay of catalases and peroxidases. *Method. Enzymol.* **1955**, *2*, 764–775.
54. Giannopolites, C.N.; Ries, S.K. Superoxide dismutase occurrence in higher plants. *Plant Physiol.* **1977**, *59*, 309–314. [CrossRef]
55. Bolger, A.M.; Lohse, M.; Usadel, B. Trimmomatic: A flexible trimmer for Illumina sequence data. *Bioinformatics* **2014**, *30*, 2114–2120. [CrossRef] [PubMed]
56. Grabherr, M.G.; Haas, B.J.; Yassour, M.; Levin, J.Z.; Amit, I. Trinity: Reconstructing a full-length transcriptome without a genome from RNA-Seq data. *Nat. Biotechnol.* **2013**, *29*, 644. [CrossRef] [PubMed]
57. Buchfink, B.; Xie, C.; Huson, D.H. Fast and sensitive protein alignment using DIAMOND. *Nat. Methods* **2015**, *12*, 59. [CrossRef] [PubMed]
58. Mistry, J.; Finn, R.D.; Eddy, S.R.; Bateman, A.; Punta, M. Challenges in homology search: HMMER3 and convergent evolution of coiled-coil regions. *Nucleic Acids Res.* **2013**, *41*, e121. [CrossRef]
59. Langmead, B.; Salzberg, S.L. Fast gapped-read alignment with Bowtie 2. *Nat. Methods* **2012**, *9*, 357–359. [CrossRef]
60. Trapnell, C.; Williams, B.A.; Pertea, G.; Mortazavi, A.; Kwan, G.; Van Baren, M.J.; Salzberg, S.L.; Wold, B.J.; Pachter, L. Transcript assembly and quantification by RNA-Seq reveals unannotated transcripts and isoform switching during cell differentiation. *Nat. Biotechnol.* **2010**, *28*, 511–515. [CrossRef]
61. Roberts, A.; Pachter, L. Streaming fragment assignment for real-time analysis of sequencing experiments. *Nat. Methods* **2013**, *10*, 71–73. [CrossRef]
62. Anders, S.; Huber, W. Differential Expression of RNA-Seq Data at the Gene Level-the DESeq Package. Available online: http://mirrors.ustc.edu.cn/bioc/3.4/bioc/vignettes/DESeq/inst/doc/DESeq.pdf (accessed on 12 January 2016).
63. Langfelder, P.; Horvath, S. WGCNA: An R package for weighted correlation network analysis. *BMC Bioinform.* **2008**, *9*, 559. [CrossRef]
64. Zhang, Y.; Zhu, L.; Xue, J.; Yang, J.; Hu, H.; Cui, J.; Xu, J. Selection and verification of appropriate reference genes for expression normalization in *Cryptomeria fortunei* under abiotic stress and hormone treatments. *Genes* **2021**, *12*, 791. [CrossRef]
65. Livak, K.J.; Schmittgen, T.D. Analysis of relative gene expression data using real-time quantitative PCR and the $2^{-\Delta\Delta ct}$ method. *Methods* **2001**, *25*, 402–408. [CrossRef]

66. Zhang, Y.; Cui, J.; Hu, H.; Xue, J.; Yang, J.; Xu, J. Integrated four comparative-omics reveals the mechanism of the terpenoid biosynthesis in two different overwintering *Cryptomeria fortunei* phenotypes. *Front. Plant Sci.* **2021**, *12*, 740755. [CrossRef] [PubMed]
67. Bajji, M.; Kinet, J.M.; Lutts. S. The use of the electrolyte leakage method for assessing cell membrane stability as a water stress tolerance test in durum wheat. *Plant Growth Regul.* **2002**, *36*, 61–70. [CrossRef]
68. Hepburn, H.A.; Naylor, R.; Stokes, D.T. Electrolyte leakage from winter barley tissue as an indicator of winter-hardiness. *Ann. Appl. Biol.* **1986**, *108*, 164–165. [CrossRef]
69. Zhou, J.; Wang, J.; Shi, K.; Xia, X.J.; Zhou, Y.H.; Yu, J.Q. Hydrogen peroxide is involved in the cold acclimation-induced chilling tolerance of tomato plants. *Plant Physiol. Biochem.* **2012**, *60*, 141–149. [CrossRef]
70. McWilliam, J.R.; Kramer, P.J.; Musser, R.L. Temperature-induced water stress in chilling-sensitive plants. *Funct. Plant Biol.* **1982**, *9*, 343–352. [CrossRef]
71. İşeri, Ö.D.; Körpe, D.A.; Sahin, F.I.; Haberal, M. Hydrogen peroxide pretreatment of roots enhanced oxidative stress response of tomato under cold stress. *Acta Physiol. Plant.* **2013**, *35*, 1905–1913. [CrossRef]
72. Lakra, N.; Nutan, K.K.; Das, P.; Anwar, K.; Singla-Pareek, S.L.; Pareek, A. A nuclear-localized histone-gene binding protein from rice (*OsHBP1b*) functions in salinity and drought stress tolerance by maintaining chlorophyll content and improving the antioxidant machinery. *J. Plant Physiol.* **2015**, *176*, 36–46. [CrossRef]
73. Ottander, C.; Campbell, D.; Oquist, G. Seasonal changes in photosystem II organisation and pigment composition in *Pinus sylvestris*. *Planta* **1995**, *197*, 176–183. [CrossRef]
74. Öquist, G.; Gardeström, P.; Huner, N.P.A. Metabolic changes during cold acclimation and subsequent freezing and thawing. In *Conifer Cold Hardiness*; Bigras, F.J., Colombo, S.J., Eds.; Springer: Dordrecht, The Netherlands, 2001; Volume 1, pp. 137–163.
75. Mochizuki, N.; Brusslan, J.A.; Larkin, R.; Nagatani, A.; Chory, J. *Arabidopsis* genomes uncoupled 5 (GUN5) mutant reveals the involvement of Mg-chelatase H subunit. *Proc. Natl. Acad. Sci. USA* **2001**, *98*, 2053–2058. [CrossRef]
76. Barber, J. Photosystem II. *Biochim. Biophys. Acta* **1998**, *1165*, 269–277. [CrossRef]
77. Malone, L.A.; Qian, P.; Mayneord, G.E.; Hitchcock, A.; Farmer, D.A.; Thompson, R.F.; Swainsbury, D.J.K.; Ranson, N.A.; Hunter, C.N.; Johnson, M.P. Cryo-EM structure of the spinach cytochrome b6f complex at 3.6 A resolution. *Nature* **2009**, *575*, 535–539. [CrossRef] [PubMed]
78. Goral, T.K.; Johnson, M.P.; Duffy, C.D.; Brain, A.P.R.; Ruban, A.V.; Mullineaux, C.W. Light-harvesting antenna composition controls the macrostructure and dynamics of thylakoid membranes in *Arabidopsis*. *Plant J.* **2012**, *69*, 289–301. [CrossRef] [PubMed]
79. Zhao, X.; Chen, T.; Feng, B.; Zhang, C.; Peng, S.; Zhang, X.; Fu, G.; Tao, L. Non-photochemical quenching plays a key role in light acclimation of rice plants differing in leaf color. *Front. Plant Sci.* **2016**, *7*, 1968–1985. [CrossRef]
80. Dixon, R.A.; Paiva, N.L. Stress-induced phenylpropanoid metabolism. *Plant Cell* **1995**, *7*, 1085. [CrossRef]
81. Vogt, T. Phenylpropanoid biosynthesis. *Mol. Plant* **2010**, *3*, 2–20. [CrossRef] [PubMed]
82. Zhang, Q.; Yang, W.; Liu, J.; Liu, H.; Lv, Z.; Zhang, C.; Chen, D.; Jiao, Z. Postharvest UV-C irradiation increased the flavonoids and anthocyanins accumulation, phenylpropanoid pathway gene expression, and antioxidant activity in sweet cherries (*Prunus avium* L.). *Postharvest Biol. Technol.* **2021**, *175*, 111490. [CrossRef]
83. Yang, J.; Guo, Z.; Zhang, Y.; Mo, J.; Cui, J.; Hu, H.; He, Y.; Xu, J. Transcriptomic profiling of *Cryptomeria fortunei* Hooibrenk vascular cambium identifies candidate genes involved in phenylpropanoid metabolism. *Forests* **2020**, *11*, 766. [CrossRef]
84. Sharma, A.; Shahzad, B.; Rehman, A.; Bhardwaj, R.; Landi, M.; Zheng, B. Response of phenylpropanoid pathway and the role of polyphenols in plants under abiotic stress. *Molecules* **2019**, *24*, 2452. [CrossRef]
85. Nakabayashi, R.; Yonekura-Sakakibara, K.; Urano, K.; Suzuki, M.; Yamada, Y.; Nishizawa, T.; Matsuda, F.; Kojima, M.; Sakakibara, H.; Shinozaki, K.; et al. Enhancement of oxidative and drought tolerance in *Arabidopsis* by overaccumulation of antioxidant flavonoids. *Plant J.* **2014**, *77*, 367–379. [CrossRef]
86. Winkel-Shirley, B. Biosynthesis of flavonoids and effects of stress. *Curr. Opin. Plant Biol.* **2002**, *5*, 218–223. [CrossRef]
87. Liu, X.; Dong, Y.; Yao, N.; Zhang, Y.; Wang, N.; Cui, X.; Li, X.; Wang, Y.; Wang, F.; Yang, J.; et al. *De novo* sequencing and analysis of the safflower transcriptome to discover putative genes associated with safflor yellow in *Carthamus tinctorius* L. *Int. J. Mol. Sci.* **2015**, *16*, 25657–25677. [CrossRef] [PubMed]
88. Song, L.; Ma, Q.; Zou, Z.; Kang, S.; Yao, Y.; Tao, J.; Kaleri, N.A.; Li, X. Molecular link between leaf coloration and gene expression of flavonoid and carotenoid biosynthesis in *Camellia sinensis* cultivar 'Huangjinya'. *Front. Plant Sci.* **2017**, *8*, 803. [CrossRef] [PubMed]
89. Bari, R.; Jones, J. Role of plant hormones in plant defence responses. *Plant Mol. Biol.* **2009**, *69*, 473–488. [CrossRef]
90. Gusta, L.V.; Trischuk, R.; Weiser, C.J. Plant cold acclimation: The role of abscisic acid. *J. Plant Growth Regul.* **2005**, *24*, 308–318. [CrossRef]
91. Lata, C.; Prasad, M. Role of DREBs in regulation of abiotic stress responses in plants. *J. Exp. Bot.* **2011**, *62*, 4731–4748. [CrossRef] [PubMed]
92. Tuteja, N. Abscisic acid and abiotic stress signaling. *Plant Signal. Behav.* **2007**, *2*, 135–138. [CrossRef] [PubMed]
93. Huang, X.S.; Liu, J.H.; Chen, X.J. Overexpression of *PtrABF* gene, a *bZIP* transcription factor isolated from *Poncirus trifoliata*, enhances dehydration and drought tolerance in tobacco via scavenging ROS and modulating expression of stress-responsive genes. *BMC Plant Biol.* **2010**, *10*, 230. [CrossRef] [PubMed]
94. Berger, S. Jasmonate-related mutants of *Arabidopsis* as tools for studying stress signaling. *Planta* **2002**, *214*, 497–504. [CrossRef]

95. Rehman, M.; Singh, Z.; Khurshid, T. Methyl jasmonate alleviates chilling injury and regulates fruit quality in 'Midknight' Valencia orange. *Postharvest Biol. Technol.* **2018**, *141*, 58–62. [CrossRef]
96. Yu, X.M.; Griffith, M.; Wiseman, S.B. Ethylene induces antifreeze activity in winter rye leaves. *Plant Physiol.* **2001**, *126*, 1232–1240. [CrossRef]
97. Pedranzani, H.; Sierra-de-Grado, R.; Vigliocco, A.; Miersch, O.; Abdala, G. Cold and water stresses produce changes in endogenous jasmonates in two populations of *Pinus pinaster* Ait. *Plant Growth Regul.* **2007**, *52*, 111–116. [CrossRef]
98. Stumpff, N.J. Ethylene Production by Loblolly Pine Seedlings during Cold Storage and Water Stress. Master's Thesis, VPISU, Blacksburg, Virginia, 1984.
99. Ramirez, V.E.; Poppenberger, B. Modes of brassinosteroid activity in cold stress tolerance. *Front. Plant Sci.* **2020**, *11*, 583666. [CrossRef] [PubMed]
100. Xu, W.; Purugganan, M.M.; Polisensky, D.H.; Antosiewicz, D.M.; Fry, S.C.; Braam, J. *Arabidopsis TCH4*, regulated by hormones and the environment, encodes a xyloglucan endotransglycosylase. *Plant Cell* **1995**, *7*, 1555–1567.
101. Davière, J.M.; Achard, P. A pivotal role of *DELLA*s in regulating multiple hormone signals. *Mol. Plant* **2016**, *9*, 10–20. [CrossRef] [PubMed]
102. Fu, X.; Richards, D.E.; Fleck, B.; Xie, D.; Burton, N.; Harberd, N.P. The *Arabidopsis* mutant sleepy1 gar2-1 protein promotes plant growth by increasing the affinity of the SCFSLY1 E3 ubiquitin ligase for DELLA protein substrates. *Plant Cell* **2004**, *16*, 1406–1418. [CrossRef] [PubMed]
103. Hirano, K.; Ueguchi-Tanaka, M.; Matsuoka, M. *GID1*-mediated gibberellin signaling in plants. *Trends Plant Sci.* **2008**, *13*, 192–199. [CrossRef] [PubMed]
104. McGinnis, K.M.; Thomas, S.G.; Soule, J.D.; Strader, L.C.; Zale, J.M.; Sun, T.P.; Steber, C.M. The *Arabidopsis SLEEPY1* gene encodes a putative F-box subunit of an SCF E3 ubiquitin ligase. *Plant Cell* **2003**, *15*, 1120–1130. [CrossRef] [PubMed]
105. Sasaki, A.; Itoh, H.; Gomi, K.; Ueguchi-Tanaka, M.; Ishiyama, K.; Kobayashi, M.; Jeong, D.; An, G.; Kitano, H.; Ashikari, M.; et al. Accumulation of phosphorylated repressor for gibberellin signaling in an F-box mutant. *Science* **2003**, *299*, 1896–1898. [CrossRef]
106. Choi, H.; Oh, E. *PIF4* integrates multiple environmental and hormonal signals for plant growth regulation in *Arabidopsis*. *Mol. Cells* **2016**, *39*, 587–593. [CrossRef]
107. Dar, A.A.; Choudhury, A.R.; Kancharla, P.K.; Arumugam, N. The *FAD2* gene in plants: Occurrence, regulation, and role. *Front. Plant Sci.* **2017**, *8*, 1789. [CrossRef]
108. Chi, X.; Yang, Q.; Pan, L.; Chen, M.; He, Y.; Yang, Z.; Yu, S. Isolation and characterization of fatty acid desaturase genes from peanut (*Arachis hypogaea* L.). *Plant Cell Rep.* **2011**, *30*, 1393–1404. [CrossRef] [PubMed]
109. Murata, N.; Ishizaki-Nishizawa, O.; Higashi, S.; Hayashi, H.; Tasaka, Y.; Nishida, I. Genetically engineered alteration in the chilling sensitivity of plants. *Nature* **1992**, *356*, 710–713. [CrossRef]
110. Kentaro, S.; Kirilov, C.N.; Sakae, T.; Imai, R. Identification of a novel LEA protein involved in freezing tolerance in wheat. *Plant Cell Physiol.* **2014**, *55*, 136–147.
111. Wise, M.J. LEAping to conclusions: A computational reanalysis of late embryogenesis abundant proteins and their possible roles. *BMC Bioinform.* **2003**, *4*, 52–70. [CrossRef]
112. Goyal, K.; Walton, L.J.; Tunnacliffe, A. LEA proteins prevent protein aggregation due to water stress. *Biochem. J.* **2005**, *388*, 151–157. [CrossRef]
113. Gao, T.; Mo, Y.; Huang, H.; Yu, J.; Wang, Y.; Wang, W. Heterologous expression of *Camellia sinensis* late embryogenesis abundant protein gene 1 (*CsLEA1*) confers cold stress tolerance in *Escherichia coli* and yeast. *Hortic. Plant J.* **2021**, *7*, 8. [CrossRef]
114. Hincha, D.K. Cryoprotectin: A plant lipid-transfer protein homologue that stabilizes membranes during freezing. *Philos. Trans. R. Soc. Lond.* **2002**, *357*, 909–916. [CrossRef]
115. Wang, L.; Zhu, W.; Fang, L.; Sun, X.; Su, L.; Liang, Z.; Wang, N.; Londo, J.P.; Li, S.; Xin, H. Genome-wide identification of *WRKY* family genes and their response to cold stress in *Vitis vinifera*. *BMC Plant Biol.* **2014**, *14*, 103. [CrossRef]
116. Zhang, T.Q.; Zhao, Y.L.; Wang, Y.C.; Liu, Z.Y.; Gao, C.Q. Comprehensive analysis of *MYB* gene family and their expressions under abiotic stresses and hormone treatments in *Tamarix hispida*. *Front. Plant Sci.* **2018**, *9*, 1303. [CrossRef]
117. Mondal, S.K.; Roy, S. Genome-wide sequential, evolutionary, organizational and expression analyses of phenylpropanoid biosynthesis associated *MYB* domain transcription factors in *Arabidopsis*. *J. Biomol. Struct. Dyn.* **2017**, *36*, 1577–1601. [CrossRef]
118. Moyano, E.; Martínez-Garcia, J.F.; Martin, C. Apparent redundancy in *MYB* gene function provides gearing for the control of flavonoid biosynthesis in antirrhinum flowers. *Plant Cell* **1996**, *8*, 1519–1532. [PubMed]
119. Yogendra, K.N.; Sarkar, K.; Kage, U.; Kushalappa, A.C. Potato *NAC43* and *MYB8* mediated transcriptional regulation of secondary cell wall biosynthesis to contain *Phytophthora infestans* infection. *Plant Mol. Biol. Rep.* **2017**, *35*, 519–533. [CrossRef]
120. Wang, N.; Liu, W.; Zhang, T.; Jiang, S.; Xu, H.; Wang, Y.; Zhang, Z.; Wang, C.; Chen, X. Transcriptomic analysis of red-fleshed apples reveals the novel role of *MdWRKY11* in flavonoid and anthocyanin biosynthesis. *J. Agric. Food Chem.* **2018**, *66*, 7076–7086. [CrossRef]
121. Zhao, C.; Liu, X.; Gong, Q.; Cao, J.; Shen, W.; Yin, X.; Grierson, D.; Zhang, B.; Xu, C.; Li, X.; et al. Three *AP2/ERF* family members modulate flavonoid synthesis by regulating type IV *chalcone isomerase* in citrus. *Plant Biotechnol. J.* **2020**, *19*, 671–688. [CrossRef] [PubMed]
122. Kashyap, P.; Deswal, R. A novel class I chitinase from *Hippophae rhamnoides*: Indications for participating in *ICE-CBF* cold stress signaling pathway. *Plant Sci.* **2017**, *259*, 62–70. [CrossRef]

123. Chen, L.; Zhong, H.; Feng, R.; Guo, Q.Q.; Hu, X.P.; Li, X.B. A novel cold-regulated gene, *COR25*, of *Brassica napus* is involved in plant response and tolerance to cold stress. *Plant Cell Rep.* **2011**, *30*, 463–471. [CrossRef] [PubMed]
124. Lin, P.; Wu, L.H.; Wei, D.H.; Chen, H.; Zhou, M.Q.; Yao, X.H.; Lin, J. Promoter analysis of cold-responsive (*COR*) gene from *Capsella bursa-pastoris* and expression character in response to low temperature. *Int. J. Agric. Biol.* **2016**, *18*, 346–352. [CrossRef]
125. Yi, Y.; Yu, X.; Ping, W. Comparison and evolution analysis of two rice subspecies *LATERAL ORGAN BOUNDARIES* domain gene family and their evolutionary characterization from *Arabidopsis*. *Mol. Phylogenet. Evol.* **2006**, *39*, 248–262.
126. Chinnusamy, V.; Zhu, J.; Zhu, J.K. Gene regulation during cold acclimation in plants. *Physiol. Plantarum* **2010**, *126*, 52–61. [CrossRef]
127. Li, T.; Yang, S.; Kang, X.; Lei, W.; Qiao, K.; Zhang, D.; Lin, H. The *bHLH* transcription factor gene *AtUPB1* regulates growth by mediating cell cycle progression in *Arabidopsis*. *Biochem. Biophys. Res. Commun.* **2019**, *518*, 565–572. [CrossRef]
128. Zhu, N.; Cheng, S.F.; Liu, X.; Du, H.; Dai, M.; Zhou, D.; Yang, W.; Zhao, Y. The *R2R3*-type *MYB* gene *OsMYB91* has a function in coordinating plant growth and salt stress tolerance in rice. *Plant Sci.* **2015**, *236*, 146–156. [CrossRef]
129. Qi, W.; Fan, S.; Wang, Q.; Chen, M.; Huang, Y.; Feng, Y.; Luo, X.; Yang, J. Rice ethylene-response *AP2/ERF* factor *OsEATB* restricts internode elongation by down-regulating a gibberellin biosynthetic gene. *Plant Physiol.* **2011**, *157*, 216–228. [CrossRef]
130. Gocal, G.F.; Sheldon, C.C.; Gubler, F.; Moritz, T.; Bagnall, D.J.; MacMillan, C.P.; Li, S.F.; Parish, R.W.; Dennis, E.S.; Weigel, D.; et al. *GAMYB*-like genes, flowering, and gibberellin signaling in *Arabidopsis*. *Plant Physiol.* **2001**, *127*, 1682–1693. [CrossRef] [PubMed]
131. Varaud, E.; Brioudes, F.; Szécsi, J.; Leroux, J.; Brown, S.; Perrot-Rechenmann, C.; Bendahmanea, M. AUXIN RESPONSE FACTOR8 regulates *Arabidopsis* petal growth by interacting with the bHLH transcription factor BIGPETALp. *Plant Cell* **2011**, *23*, 973–983. [CrossRef]
132. Van den Broeck, L.; Dubois, M.; Vermeersch, M.; Storme, V.; Matsui, M.; Inzé, D. From network to phenotype: The dynamic wiring of an Arabidopsis transcriptional network induced by osmotic stress. *Mol. Syst. Biol.* **2017**, *13*, 961. [CrossRef]
133. Colebrook, E.H.; Thomas, S.G.; Phillips, A.L.; Hedden, P. The role of gibberellin signaling in plant responses to abiotic stress. *J. Exp. Biol.* **2014**, *217*, 67–75. [CrossRef] [PubMed]
134. Kazan, K. Diverse roles of jasmonates and ethylene in abiotic stress tolerance. *Trends Plant Sci.* **2015**, *20*, 219–229. [CrossRef]
135. Nolan, T.M.; Brennan, B.; Yang, M.R.; Chen, J.N.; Zhang, M.C.; Li, Z.H.; Wang, X.L.; Bassham, D.C.; Walley, J.; Yin, Y.H. Selective autophagy of BES1 mediated by DSK2 balances plant growth and survival. *Dev. Cell* **2017**, *41*, 33–46. [CrossRef]
136. Wan, Y.; Schwaninger, H.; Li, D.; Simon, C.; Wang, Y.; He, P. The eco-geographic distribution of wild grape germplasm in China. *VITIS* **2008**, *47*, 77.
137. Xu, W.; Li, R.; Zhang, N.; Ma, F.; Jiao, Y.; Wang, Z. Transcriptome profiling of *Vitis amurensis*, an extremely cold-tolerant Chinese wild *Vitis* species, reveals candidate genes and events that potentially connected to cold stress. *Plant Mol. Biol.* **2014**, *86*, 527–541. [CrossRef] [PubMed]
138. Yun, J.G.; Hayashi, T.; Yazawa, S.; Katoh, T.; Yasuda, Y. Acute morphological changes of palisade cells of *Saintpaulia* leaves induced by a rapid temperature drop. *J. Plant Res.* **1996**, *109*, 339–342. [CrossRef]
139. Kratsch, H.; Wise, R. The ultrastructure of chilling stress. *Plant Cell Environ.* **2000**, *23*, 337–350. [CrossRef]
140. Zhuang, Q.; Chen, S.; Jua, Z.; Yao, Y. Joint transcriptomic and metabolomic analysis reveals the mechanism of low temperature tolerance in *Hosta ventricosa*. *PLoS ONE* **2021**, *16*, e0259455. [CrossRef]
141. Yang, X.; Zhao, T.; Rao, P.; Gao, K.; Yang, X.; Chen, Z.; An, X. Transcriptome profiling of *Populus tomentosa* under cold stress. *Ind. Crop. Prod.* **2019**, *135*, 283–293. [CrossRef]
142. Lu, C.; Yin, L.; Li, K. Proteome expression patterns in the stress tolerant evergreen *Ammopiptanthus nanus* under conditions of extreme cold. *Plant Growth Regul.* **2010**, *62*, 65–70. [CrossRef]
143. Kaplan, F.; Kopka, J.; Haskell, D.W.; Zhao, W.; Schiller, K.C.; Gatzke, N.; Sung, D.Y.; Guy, C.L. Exploring the temperature-stress metabolome of *Arabidopsis*. *Plant Physiol.* **2004**, *136*, 4159–4168. [CrossRef]
144. Jin, J.; Zhang, H.; Zhang, J.; Liu, P.; Chen, X.; Li, Z.; Xu, Y.; Lu, P.; Cao, P. Integrated transcriptomics and metabolomics analysis to characterize cold stress responses in *Nicotiana tabacum*. *BMC Genom.* **2017**, *18*, 496. [CrossRef]
145. Guy, C.; Kaplan, F.; Kopka, J.; Selbig, J.; Hincha, D.K. Metabolomics of temperature stress. *Physiol. Plant.* **2008**, *132*, 220–235. [CrossRef]
146. Peng, Y.; Lin, W.L.; Wei, H.; Krebs, S.L.; Arora, R. Phylogenetic analysis and seasonal cold acclimation-associated expression of early light-induced protein genes of *Rhododendron catawbiense*. *Physiol. Plant.* **2008**, *132*, 44–52. [CrossRef]
147. Gage, K.; Jens, R.; Wilson, R.C.; Kopka, J.; Erban, A.; Winge, P.; Bones, A.M.; Davik, J.; Alsheikh, M.K.; Randall, S.K. Integrative "omic" analysis reveals distinctive cold responses in leaves and roots of strawberry, *Fragaria* × *ananassa* 'Korona'. Fron. *Plant Sci.* **2015**, *6*, 826.
148. Maruyama, K.; Urano, K.; Yoshiwara, K.; Morishita, Y.; Sakurai, N.; Suzuki, H.; Kojima, M.; Sakakibara, H.; Shibata, D.; Saito, K.; et al. Integrated analysis of the effects of cold and dehydration on rice metabolites, phytohormones, and gene transcripts. *Plant Physiol.* **2014**, *164*, 1759–1771. [CrossRef] [PubMed]